Development of macrophage-targeted therapy using peptide/protein-loaded extracellular vesicles

2022

Misako Takenaka

Preface

Macrophages are innate immune cells derived from monocytes involved in tissue homeostasis. Recent years, uncontrolled activation of macrophages has been recognized to induce the onset and progression of various diseases such as autoimmune diseases, metabolic disease, and cancer [1]. Development of macrophage-targeted therapeutics, which can effectively regulate macrophage function, can be a promising treatment option for those various diseases.

Extracellular vesicles (EVs) are released by cells of almost all types of living organism including human, animal, plant, and microorganism [2,3]. EVs can be divided into small EVs (sEVs), microvesicles (MVs)/ large EVs (lEVs), and apoptotic bodies. sEVs and lEVs enclose endogenous proteins and nucleic acids derived from their parental cells, and play important roles as carriers in intercellular communication by delivering enclosed cargoes to recipient cells [4,5]. Because of their intrinsic nature as endogenous delivery carriers, EVs are considered as a novel candidate of drug delivery system (DDS). Researchers have revealed that systemically administered sEVs were mostly taken up by macrophages through the recognition of EV's physicochemical properties (e.g. size and membrane charge) [6,7], which indicates that sEVs can be a potent drug delivery carrier to macrophages. Compared to sEVs, there was less information on pharmacokinetics of lEVs, however given the large size and negative membrane charge of lEVs [8], it was speculated that lEVs could also be applied to macrophage targeting therapy. Moreover, bioactive molecules such as peptides and proteins can be easily loaded to EVs by genetic engineering [9], which can save complicated process for manufacturing drug-containing vehicle. These unique properties of EVs would be the rationale for the development of macrophage-targeted EV-based therapeutics.

I attempted to establish macrophage delivery system of therapeutic peptide or proteins using sEVs and lEVs. Since it was considered that drug loading to the inner space of EVs was suitable for intracellular drug delivery, while drug loading to outer membrane of EVs was suitable for targeting extracellular molecules (e.g. extracellular receptors), I developed EVs which internally or externally loaded with peptides /proteins depending on the localization of target molecules. Then, I investigated the potential of EVs as delivery carriers targeting extracellular and intracellular molecules of macrophages.

Table of Contents

Chapter 1

Development of synovial macrophage-targeted, anti-arthritis therapy based on IL-4 delivery by sEVs

I-1 Introduction

In inflammatory diseases, M1-polarlized macrophages largely contribute to the onset and progression of the diseases by producing pro-inflammatory mediators [10]. The anti-inflammatory strategy of suppressing these mediators, such as IL-6 or TNFα, has already been applied [11,12] However, considering the critical role of macrophages, an approach that directly suppresses M1 activation and promotes M2 activation of macrophages could be a more efficient treatment against chronic inflammatory diseases, in which various pro-inflammatory mediators are inhibited at once and wound healing is accelerated by anti-inflammatory mediators secreted by M2 macrophages [13].

Interleukin-4 (IL4), a Th2-derived cytokine, can induce M2 macrophages [14]. Owing to its immunomodulatory activity, studies have been carried out to develop an anti-inflammatory therapy utilizing IL4 [15,16]. However, there are still problems in the development of IL4 therapy, such as insufficient anti-inflammatory effects [17–20] and undesirable side effects [21–24], due to the low delivery efficiency to target cells, macrophages. Since sEVs are efficiently recognized and taken up by macrophages through the negative charges of their membrane, derived from phosphatidylserine (PS) [6,7], it was expected that sEV would be a promising IL4 delivery carrier to macrophages.

Moreover, the localization of the IL4 receptor (IL4R) to the early endosome (EE) and subsequent stabilization of the IL4R heterodimer in the EE contribute to full activation and duration of IL4 signaling [25,26]. As sEVs are taken up by macrophages mostly through endocytosis [27], I assumed that IL4 loaded sEVs promote the localization of IL4R into EE, followed by amplification of IL4 signal transduction.

Therefore, I hypothesized that IL4 loaded sEVs could be a potent therapeutic agent for inflammatory diseases, which improve the target-cell specificity and bioactivity of IL4. In this chapter, I prepared IL4 loaded sEVs (IL4-sEVs) by constructing plasmid DNA expressing a fusion protein of IL4 and sEV-tropic protein, lactadherin (LA), and isolating from HEK293 cells transfected with the plasmid DNA. Subsequently, anti-inflammatory effects were evaluated using both M1-polarlized macrophage cell line and animal model of rheumatoid arthritis, a serious inflammatory disease.

I-2 Materials & Methods

Cell culture

Murine macrophage cell line RAW264.7 cells were purchased from American Type Culture Collection (ATCC) and cultured in 10% fetal bovine serum (FBS)-containing RPMI 1640 (Nissui Co. Ltd., Japan). Human Embryonic Kidney 293 (HEK293) cells purchased from ATCC (CRL-1573) were

cultured in 10%-FBS-containing Dulbecco's modified Eagle's medium (Nissui Co. Ltd.). Macrophage scavenger receptor 1 (MSR1) gene knockout RAW264.7 cells were constructed as previously described [28]. Briefly, RAW264.7 cells were transfected with a complex of MSR1-targeted crRNA, tracrRNA, and Cas9. The MSR1 knockout of CRISPR/Cas9-treated cell clones was confirmed by western blotting using an anti-MSR-A1/MSR1 antibody. MSR1 gene knockout RAW264.7 cells were cultured in 10%-FBS-containing RPMI 1640 (Nissui Co. Ltd.).

Animals

Eight-week-old male DBA/1J mice were purchased from Japan SLC Inc. (Japan). The mice were housed in polycarbonate cages and fed standard mouse chow and water ad libitum. All protocols for the animal experiments were approved by the Animal Experimentation Committee of the Kyoto University Graduate School of Pharmaceutical Sciences.

Construction of plasmid DNA

The coding sequence of the sEV-tropic protein, LA, was obtained as described previously [29]. The IL4 coding sequence was synthesized by Integrated DNA Technologies (USA). The IL4 encoding sequence was synthesized along with the LA sequence using a two-step polymerase chain reaction (PCR) method to obtain IL4-LA. The IL4-LA encoding fusion protein was inserted into the Hind III/NheI site of the pcDNA3.1 vector (Thermo Fisher Scientific, USA) to construct pCMV-IL4-LA.

The gene sequence encoding Gag was obtained, as described in previous reports [30]. The Gag encoding sequence was fused with the IL4 sequence using a two-step polymerase chain reaction (PCR) method to obtain Gag-IL4. The Gag-IL4 encoding fusion protein was inserted into the EcoR1/Not1 site of the pcDNA3.1 vector to construct pCMV-Gag-IL4.

Isolation of sEVs

HEK293 cells were transfected with pCMV-IL4-LA or pCMV-Gag-IL4 using PEI Max (Polysciences, Inc., USA), as described previously [31]. The culture media of nontransfected and transfected cells were collected and cleared by successive centrifugation steps (300 × *g* for 10 min, 2000 × *g* for 20 min, 10000 × *g* for 30 min) to remove cellular debris and large vesicles, followed by filtration through a 0.2-μm syringe filter. The filtrated sample was then ultracentrifuged twice at 100000 × *g* for 1 h and the pellets were washed with phosphate buffered saline (PBS) and resuspended in PBS. The amount of isolated sEVs was estimated by measuring the protein concentration using the

Bradford assay.

Cell treatment

For M1 polarization of RAW264.7 cells, 10 ng/mL LPS (Sigma-Aldrich, USA) and 10 ng/mL IFNγ (Cell Guidance Systems, UK) were added to the cells and incubated for 6 h. The cell culture medium was then replaced with Opti-MEM (Thermo Fisher Scientific, USA) and treated with control sEVs, 20 ng/mL or 60 ng/mL IL4 (Cell Guidance Systems, UK), Gag-IL4 sEVs (IL4 concentration: 20 ng/mL) or IL4-sEVs (IL4 concentration: 20 or 60 ng/mL) for 24 h. In the endocytosis inhibition assay, 1 μM of Cytochalasin D (Wako Pure Chemicals Industries, Ltd., Japan), an actin polymerization inhibitor, was added to M1-polarized RAW264.7 cells 30 min before the addition of sEVs.

CIA induction and treatment

At 9 weeks of age, mice were used to establish collagen-induced arthritis (CIA) model. CIA induction and treatment were carried out under anesthesia with three types of mixed anesthetic agents. The anesthetic agents were prepared with 0.3 mg/kg medetomidine (Domitor, Zenoaq, Japan), 4.0 mg/kg midazolam (Sandoz, Japan), and 5.0 mg/kg butorphanol (Vetorphale, Meiji Seika Pharma Co., Ltd., Japan) and were administered to the mice by intraperitoneal injection. Mice were immunized intradermally at the base of the tail with 100 μg of chicken-type II collagen (Sigma-Aldrich) emulsified in complete Freund's adjuvant, containing M. tuberculosis H37Ra (Chondrex, USA), on day 0 and day 21 as a booster injection. After the onset of arthritis on day 26, the CIA mice were randomly divided into four groups with six mice: PBS group, control-sEVs group, IL4 group, and IL4-sEVs group. Three nonimmunized mice were allocated to the normal control group.

PBS, control-sEVs (1 μg), IL4 (3 ng), or IL4-sEVs (containing 3 ng of IL4) were intraarticularly injected into each ankle joint of the CIA mice once daily from day 27 to day 36. The mice were sacrificed on day 37, and then serum and ankle joint tissues were collected.

Evaluation of the severity of arthritis

The severity of arthritis was monitored every other day using two clinical parameters: clinical score and paw thickness. Each hind paw was scored individually as follows: 0 = no obvious differences in appearance vs. healthy control mice, 1 = one or two toes inflamed and swollen (no apparent swelling of paw or ankle), 2 = three or more toes inflamed and swollen, but no paw swelling, or mild swelling of the entire paw, 3 = swelling of the entire paw, 4 = severe swelling of the entire paw and all toes.

The clinical score was the sum of the scores for each hind paw, with a maximum clinical score of 8 per animal. The paw swelling was assessed by measuring the hind paw thickness using a caliper.

Western blot analysis

Cell lysates were prepared by freezing and thawing cycles in the presence of a protease inhibitor cocktail (Nacalai Tesque Inc., Japan), followed by centrifugation at 15000 × *g* for 15 min. The protein concentration was measured using the Bradford assay. sEVs or cell lysates were reduced by 100 mM dithiothreitol and heat treatment at 95 °C for 3 min and separated on an 8% sodium dodecyl sulfate–polyacrylamide gel through sodium dodecyl sulfate polyacrylamide gel electrophoresis (SDS-PAGE). The proteins were then transferred from the gel to a polyvinylidene fluoride membrane. After blocking with Blocking One reagent (Nacalai Tesque Inc.), the membranes were incubated with the following primary antibodies for 1 h at room temperature or overnight at 4 °C: rabbit anti-HSP70 antibody (1:1000; Cell Signaling Technology, USA), rabbit anti-CD81 antibody (1:200; Santa Cruz Biotechnology, USA), mouse anti-Alix antibody (1:200; Santa Cruz Biotechnology), rabbit anti-Calnexin antibody (1:1000; Santa Cruz Biotechnology), rat anti-IL4 antibody (1:2000; GeneTex, USA), rabbit anti-iNOS antibody (1:2000; Abcam, USA), mouse anti-Arg1 antibody (1:200; Santa Cruz Biotechnology), and rabbit anti-GAPDH antibody (1:10000; Abcam). The membranes were then incubated with the following horseradish peroxidase (HRP)-conjugated secondary antibodies for 1 h at room temperature: goat anti-rabbit IgG-HRP (1:1000; Cell Signaling Technology), horse anti-mouse IgG-HRP (1:1000; Cell Signaling Technology), and goat anti-rat IgG-HRP (1:5000; Santa Cruz Biotechnology). The membranes were washed three times and reacted with an Immobilon Western Chemiluminescent HRP substrate (Merck Millipore, USA). The chemiluminescence was detected using LAS-3000 instrument (Fujifilm, Japan).

Transmission electron microscopy (TEM) observation

sEVs were fixed in 4% paraformaldehyde and added to a Carbon/Formvar-film-coated TEM grid (Okenshoji, Japan) for 20 min. After washing with PBS, the samples were treated with 1% glutaraldehyde for 5 min and washed four times with distilled water. They were then stained with 1% uranyl acetate for 2 min and observed using TEM (Hitachi H-7650, Hitachi High-Technologies Corporation, Japan).

Measurement of the zeta potential

sEVs were mixed with distilled water and added to the disposable folded capillary cells. The zeta potential of the sEVs was measured using a Zetasizer Nano ZS (Malvern Instruments, UK).

Enzyme-linked immunosorbent assay (ELISA)

IL4 concentrations in the samples were measured using mouse IL4 ELISA OptEIA^{TM} sets (Pharmingen, USA) according to the manufacturer's instructions. The levels of TNF-α in the cell culture supernatants or ankle joint tissues were determined using mouse TNF-α ELISA OptEIA^{TM} sets (Pharmingen) according to the manufacturer's instructions. The levels of IL-6 in ankle joint tissues were measured using IL-6 ELISA OptEIA^{TM} sets (Pharmingen) according to the manufacturer's instructions.

mRNA extraction and quantitative real-time polymerase chain reaction (qRT-PCR) analysis

Cells or ankle joint tissues were homogenized in Sepasol RNA-I Super G (Nacalai Tesque Inc.) and total RNA was extracted according to the manufacturer's instructions. The RNA concentration was determined using a Nanodrop 2000 spectrophotometer (Thermo Fisher Scientific Inc.). Complementary DNA (cDNA) was synthesized using ReverTra Ace qPCR RT Kit with gDNA Remover (Toyobo Co. Ltd., Japan), according to the manufacturer's instructions. cDNA was used as a template for amplifying genes by the qRT-PCR analysis using Step One Plus (Applied Biosystems Inc., USA). The used primers are listed in Table 1. PCR was performed using the following cycling conditions: 40 cycles at 95 °C for 3 s, 60 °C for 15 s, and 72 °C for 15 s. To quantify isolated RNA and measure the cDNA synthesis efficiency, the levels of target cDNAs were normalized to the expression level of the endogenous reference gene, glyceraldehyde-3-phosphate dehydrogenase (GAPDH).

Table 1 Primer sequences used in the RT-qPCR analysis

Gene name	Forward primer	Reverse primer
GAPDH	AGGTCGGTGTGAACGGATTTG	TGTAGACCATGTAGTTGAGGTCA
Arg1	CAGAAGAATGGAAGAGTCAG	CAGATATGCAGGGAGTCACC
CD206	TGCAAGGATCATACTTCCCT	TGATGTTCTCCAGTAGCCAT
iNOS	GTTCTCAGCCCAACAATACAAGA	GTGGACGGGTCGATGTCAC
CXCL10	AAGTGCTGCCGTCATTTTCT	CCTATGGCCCTCATTCTCAC
IL1β	CCCAAGCAATACCCAAAGAA	CATCAGAGGCAAGGAGGAAA
IL12	ACTCCCCATTCCTACTTCTCC	CATTCCCGCCTTTGCATTG
IL10	GGAGCAGGTGAAGAGTGATTT	TCCAAGGAGTTGTTTCCGTTAG
TGFβ	CTCCCGTGGCTTCTAGTGC	GCCTTAGTTTGGACAGGATCTG
IL4	ACAGGAGAAGGGACGCCAT	GAAGCCCTACAGACGAGCTCA

Measurement of nitrite (NO) concentration

The cell culture supernatants were collected and the NO concentration was determined using the Griess Reagent Kit (Biotium, USA), according to the manufacturer's instructions. Samples were analyzed using a plate reader (Multiskan, Fisher Scientific Inc.) by measuring the absorbance (optical density (OD) 570 nm/OD 620 nm).

Flow cytometry

The sEVs were stained using the PKH67 green fluorescent cell linker kit (Sigma-Aldrich), as described previously [32]. Briefly, sEVs were mixed with 2-μM PKH67 dye prepared in Diluent C and incubated for 5 min at 25 °C. The staining reaction was stopped by adding 5% bovine serum albumin (BSA) prepared in PBS. The samples were ultracentrifuged at 100000 × *g* for 1 h to remove the free PKH67 dye. After washing the pellets with PBS, they were resuspended in PBS and PKH67-labeled sEVs were prepared. M1 macrophages (wild-type and MSR1-knockout RAW264.7 cells) were cultured overnight in a 96-well plate and replaced with Opti-MEM (Thermo Fisher Scientific Inc.). PKH67-labeled sEVs were added to the cells at a concentration of 10 μg/mL, followed by incubation for 4 h at 37 °C. The cells were washed three times with PBS, and then suspended in PBS. The cellular uptake of PKH67-labeled sEVs was determined using a Gallios Flow Cytometer (Beckman Coulter, USA) according to the manufacturer's instructions. Data were analyzed using the Kaluza software (Beckman Coulter) to determine the mean fluorescence intensity (MFI).

Confocal microscopy analysis

Cells were replaced with Opti-MEM and control-sEVs, IL4, or IL4-sEVs (IL4 concentration: 60 ng/mL) were added. After 4 h of incubation, the cells were washed with PBS and fixed with 4% paraformaldehyde for 20 min. A membrane permeation treatment was performed using PBS containing 0.25% Triton X-100 (Nacalai Tesque Inc.). After 10 min of incubation, the cells were washed with PBS for 5 min and incubated with 1% BSA plus 22.52 mg/mL glycine in PBS-t (PBS plus 0.1% Tween 20) for 30 min to block nonspecific binding of the antibodies. The cells were then reacted with the primary antibody (anti-IL4Rα antibody (1:80 dilution), Santa Cruz Biotechnology; EEA1 antibody (1:300 dilution), Abcam) overnight at 4 °C. The cells were then washed with PBS and incubated with the secondary antibody (goat anti-mouse IgG H&L (Alexa Fluor 488) (1: 700 dilution), Abcam; goat anti-rabbit IgG H&L (Alexa Fluor 647) (1:700 dilution), Abcam) for 1 h at room temperature. After washing, 300 nM 4′,6′-diamidino-2-phenylindole (DAPI) was added for 5 min and Fluoro-KEEPER Antifade Reagent (Nacalai Tesque Inc.) was applied to the coverslips. The samples were observed using a confocal microscope (A1R MP; Nikon Instech Co. Ltd., Japan).

Histological staining assessment

Hind ankle joint tissues were fixed in 10% neutral-buffered formalin (Nacalai Tesque Inc.) at 25 °C for 48 h and the samples were decalcified in 0.5 mol/L EDTA (Wako Pure Chemicals Industries, Ltd.) for 14 days. After dehydration, the specimens were embedded in paraffin (Paraplast Plus, McCormick Scientific, USA) and 4-μm-thick sagittal sections were stained with hematoxylin–eosin (H&E) and observed under a microscope (Biozero BZ-8000, KEYENCE, Japan). Histopathological scoring was performed by assessing three parameters: synovitis, pannus formation, and cartilage and bone destruction at four grades (0–3: 0 = normal, 1 = mild, 2 = moderate, and 3 = severe).

Immunohistochemical analysis

Hind ankle joint tissues were harvested and fixed in 4% paraformaldehyde (Nacalai Tesque Inc.) at 4 °C for 48 h. The samples were decalcified in 0.5 mol/L EDTA (Wako Pure Chemicals Industries, Ltd.) for 14 days. The specimens were placed in 10% sucrose solution for 24 h, in 15% sucrose solution for another 24 h, and subsequently in 20% sucrose solution for 24 h at 4 °C, embedded in optimal cutting temperature (OCT) compound (Sakura Finetek Japan Co. Ltd., Japan), and frozen. The frozen specimens were cut into 4-μm-thick sagittal sections, which were fixed with 4% paraformaldehyde for 20 min. The samples were washed with PBS for 5 min and incubated with 20% BSA in PBS at

37 °C to avoid nonspecific binding of the antibodies. After 1 h of incubation, the samples were incubated with the primary antibody (anti-CD86 antibody, 1:50, Santa Cruz Biotechnology, USA; anti-CD206 antibody, 1:100, Sigma-Aldrich, USA) for 1 h at 37 °C. The samples were then washed with PBS and stained with the secondary antibody (goat anti-mouse IgG H&L (Alexa Fluor 647) 1:500, Abcam, USA; goat anti-rabbit IgG H&L (Alexa Fluor 488), 1:500, Abcam) for 1 h at 37 °C. After washing, 300-nM DAPI was added to the samples for 5 min and Fluoro-KEEPER Antifade Reagent (Nacalai Tesque Inc.) was applied to the coverslips. The samples were observed under a microscope (Biozero BZ-8000, Keyence).

Statistical analysis

Statistical differences were evaluated using a one-way analysis of variance, followed by Tukey–Kramer multiple comparison test; $p < 0.05$ was considered statistically significant.

I-3 Results

I-3-a Construction of IL4-LA coding plasmid DNA and isolation of IL4 loaded sEVs from HEK293 cells transfected with pCMV-IL4-LA.

pCMV-IL4-LA, a plasmid DNA encoding a fusion protein of IL4 and LA, was constructed to obtain IL4 loaded sEVs (IL4-sEVs; Fig. 1a). pCMV-Gag-IL4, a plasmid DNA encoding a fusion protein of Gag and IL4, was also constructed to encapsulate IL4 inside of sEV (Gag-IL4 sEVs; Fig. 1a) as a control of IL4 loading method. A Western blot analysis indicated that control-sEVs, isolated from nontransfected HEK293 cells, Gag-IL4 sEVs and IL4-sEVs contained sEV marker proteins, Alix, HSP70, and CD81 (Fig. 1b). The endoplasmic reticulum marker, calnexin, was not present in both sEV samples, which suggests that they were not contaminated with cell debris (Fig. 1b). A Western blot analysis confirmed that IL4 was successfully loaded to sEVs (Fig. 1c). The amount of IL4 loaded to single IL4-sEV was estimated approximately 3.8 ng IL4/μg sEV by ELISA.

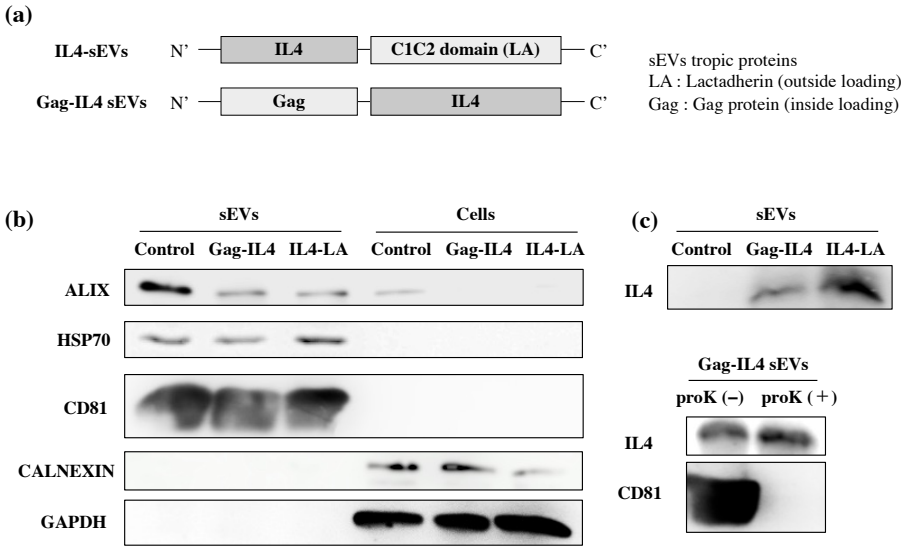

Fig. 1 Confirmation of the collection of IL4-sEVs from HEK293 cells transfected with pCMV-IL4-LA.
(a) IL4-LA and Gag-IL4 coding plasmid DNAs were designed. (b) Western blot analysis of Alix, HSP70, CD81, calnexin and GAPDH in sEVs and cell lysates. (c) Western blot analysis of IL-4 in control-sEVs, Gag-IL4 sEVs and IL4-sEVs. Inner loading of IL-4 was confirmed by Western blotting of Gag-IL4 sEVs with/ without protease K (proK) treatment using IL-4 or CD81 antibodies.

I-3-b IL4 loading to sEVs hardly changed physicochemical properties of sEVs.

The morphology and zeta potential of the sEVs were investigated using TEM and zetasizer, respectively. TEM images and histograms of particle size distribution showed that the morphologies of control-sEVs and IL4-sEVs were almost the same (Fig. 2a, b). The zeta potential of the sEVs was approximately -30 mV, irrespective of the IL4 loading (Fig. 2c). These results suggest that the loading of IL4 to sEVs had a small effect on the physicochemical properties of sEVs.

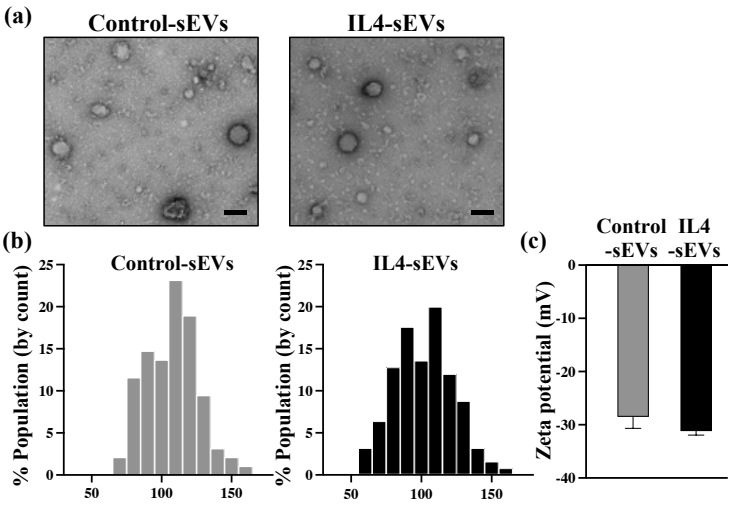

Fig. 2 Physicochemical properties of sEVs.
(a) TEM images of control-sEVs and IL4-sEVs. Scale bar = 100 nm. (b) Histograms of particle size distribution of control-sEVs and IL4-sEVs. (c) Zeta potentials of control-sEVs and IL4-sEVs.
The results are expressed as means ± standard deviation (n = 3).

I-3-c IL4-sEVs greatly suppressed pro-inflammatory mediator expressions in M1 macrophages and upregulated the expression levels of M2 marker genes.

The ability of IL4-sEVs to inhibit the pro-inflammatory cytokine, chemokine, and inducible nitric oxide synthase (iNOS)/NO production in M1-polarized RAW264.7 cells M1-polarized RAW264.7 cells M1-polarized RAW264.7 cells M1-polarized RAW264.7 cells was evaluated. As shown in Fig. 3a, the TNFα concentration in the supernatant of cells treated with IL4 or IL4-sEVs was significantly lower than that of nontreated cells (NT). Since Gag-IL4 sEVs had no inhibitory effects on TNF-α production from M1 macrophages, they were excluded from further analysis. The mRNA expression level of CXCL10 was also decreased by the treatment with IL4 or IL4-sEVs in a concentration-dependent manner (Fig. 3b). Furthermore, the suppressive effects of IL4-sEVs (60 ng/mL) on both pro-inflammatory mediators were larger than those of the same concentration of IL4. iNOS mRNA and protein expressions were significantly down-regulated when M1 macrophages were treated with IL4 or IL4-sEVs (Fig. 3c, d). The NO production in M1 macrophages was also reduced by the treatment (Fig. 3e), which corresponded to the results of iNOS expression.

Subsequently, I investigated expressions of M2 marker genes, Arginase1 (Arg1) and Mannose receptor (CD206), in M1 macrophages after the treatment with IL4-sEVs. The mRNA (Arg1 and CD206) and protein (Arg1) expressions were largely increased by the treatment with IL4 or IL4-sEVs (Fig. 3f–h).

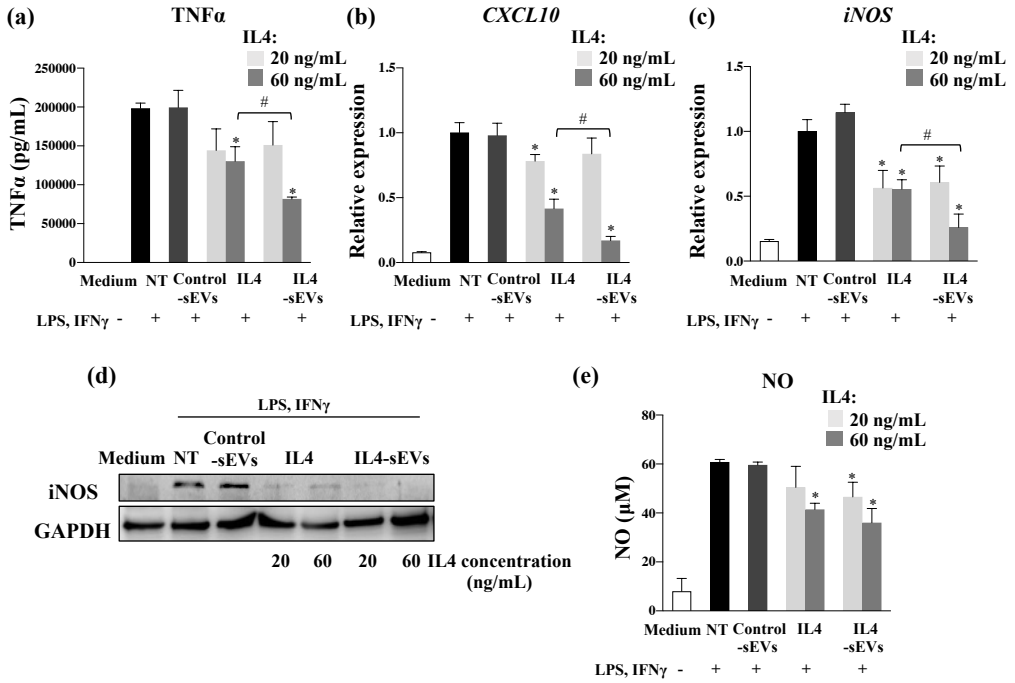

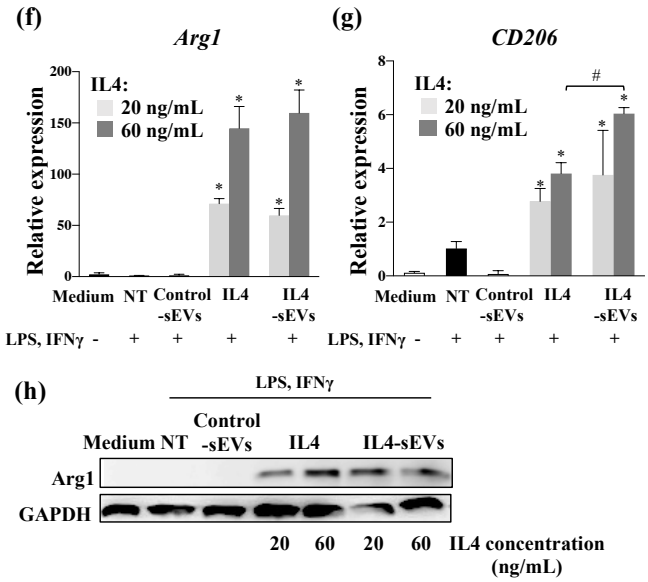

Fig. 3 Suppression and inducing effect of IL4-sEVs on the expression of M1 and M2 marker genes in RAW264.7 cells.
Expression of pro-inflammatory and anti-inflammatory mediators in nontreated M1 macrophages (NT) and M1 macrophages treated with control-sEVs, Gag-IL4 sEVs, IL4, or IL4-sEVs (IL4: 20 or 60 ng/mL). (a) TNFα concentration in the culture media (b) CXCL10 mRNA (c) iNOS mRNA (d) iNOS and GAPDH (as an internal control) proteins in cell lysates (e) Nitrite concentrations in the culture media (f), (g) Arg1 and CD206 mRNA (h) Arg1 and GAPDH (as an internal control) proteins in cell lysates
The results are expressed as the mean ± standard deviation ($n = 4$). *$P < 0.05$, compared to the nontreated (NT) group. #$P < 0.05$, compared to the IL4 group.

I-3-d Inhibition of sEV uptake by macrophages abolished the anti-inflammatory activity of IL4-sEVs.

Further, I investigated whether IL4 receptor (IL4R) endocytosis is essential for IL4 signaling in macrophages by inhibiting their endocytosis using Cytochalasin D and evaluating the anti-inflammatory effects of IL4 and IL4-sEVs on M1 macrophages. As shown in Fig. 4a–c, in the presence of Cytochalasin D, both IL4 and IL4-sEVs did not exhibit inhibitory effect on iNOS, an M1 marker, or induction effect on Arg1, an M2 marker. These results indicate that IL4R endocytosis is necessary for the transduction of IL4 signaling in macrophages and regulation of M1/M2 polarization by IL4 and IL4-sEVs.

Further, I evaluated the anti-inflammatory effects of IL4 and IL4-sEVs in macrophages with reduced sEV uptake abilities. MSR1, which recognizes various negatively charged ligands [33], has a major role in the uptake of sEV by RAW264.7 macrophages [34]. Therefore, it was assumed that, using MSR1-knockout RAW264.7 cells, I could evaluate the anti-inflammatory effects of IL4-sEVs under the condition of a reduced uptake of sEVs by macrophages. The sEV uptake by wild-type or MSR1-knockout M1 macrophages was investigated by flow cytometry. FITC-dextran was used as a

marker for nonspecific fluid-phase endocytosis or macropinocytosis by macrophages [35]. The uptake of PKH67-labeled sEVs was reduced in MSR1-knockout M1 macrophages compared to that in wild-type M1 macrophages, while the uptake of FITC-dextran was comparable (Fig. 4d). Subsequently, M1 and M2 marker expressions in wild-type or MSR1-knockout RAW264.7 cells after the treatment with IL4 or IL4-sEVs were assessed. As shown in Fig. 4e–g, the gene and protein expression levels of iNOS and Arg1 in MSR1-knockout macrophages treated with IL4 were comparable to those in wild-type macrophages treated with IL4. On the other hand, the MSR1-knockout macrophages treated with IL4-sEVs exhibited higher expression of iNOS and lower expression of Arg1, compared to those of the wild-type macrophages. These results suggest that the uptake of IL4-sEVs by macrophages through the recognition of sEV physicochemical properties was necessary for IL4-sEVs to exhibit the high anti-inflammatory effects.

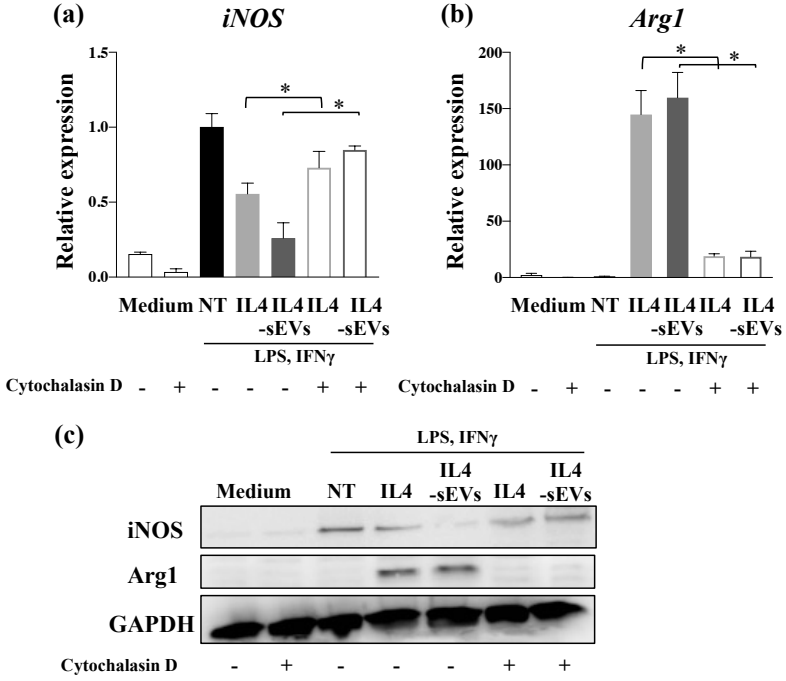

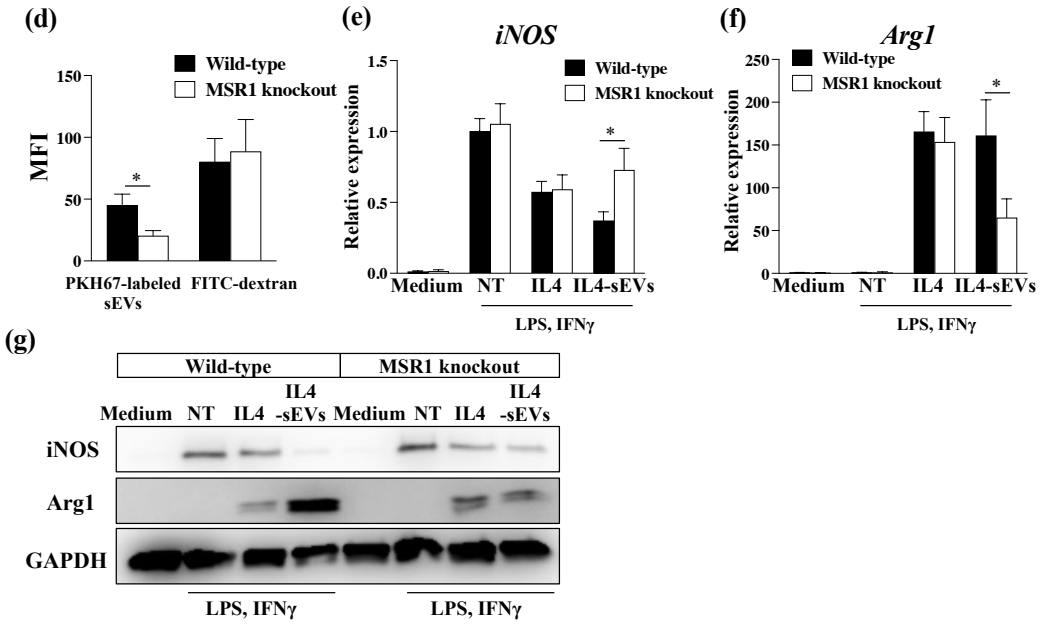

Fig. 4 Effect of endocytosis inhibition on the anti-inflammatory effect of IL4 and IL4-sEVs against M1 macrophages.
(a), (b) iNOS and Arg1 mRNA expressions in M1 macrophages treated with IL4 or IL4-sEVs (IL4: 60 ng/mL) with or without Cytochalasin D. **P* < 0.05 vs that with Cytochalasin D. The results are expressed as the mean ± standard deviation (*n* = 4). (c) Western blot analysis of iNOS, Arg1, and GAPDH (as an internal control) in M1 macrophages treated with IL4 or IL4-sEVs with or without Cytochalasin D. (d) sEV and FITC-dextran uptake by wild-type or MSR1 gene knockout RAW264.7 cells. MFI: Mean Fluorescence Intensity (e), (f) iNOS and Arg1 mRNA expressions in wild-type or MSR1-knockout M1 macrophages treated with IL4 or IL4-sEVs. **P* < 0.05 vs MSR1-knockout M1 macrophages. The results are expressed as the mean ± standard deviation (*n* = 4). (g) Western blot analysis of iNOS, Arg1, and GAPDH (as an internal control) in wild-type or MSR1-knockout M1 macrophages treated with IL4 or IL4-sEVs.

I-3-e

Endosomal localization of IL4Rα in macrophages increased by adding IL4-sEV.

The localization of IL4Rα (IL4 receptor α) in M1 macrophages after the addition of control-sEVs, IL4, or IL4-sEVs was observed. Confocal microscopy images showed that IL4Rα and early endosome antigen 1 (EEA1) in macrophages colocalized more frequently in RAW264.7 cells added with IL4-sEVs than that in the cells added with IL4 (Fig. 5a, b). This result supports the hypothesis that IL4-sEVs promoted IL4R endocytosis compared to IL4.

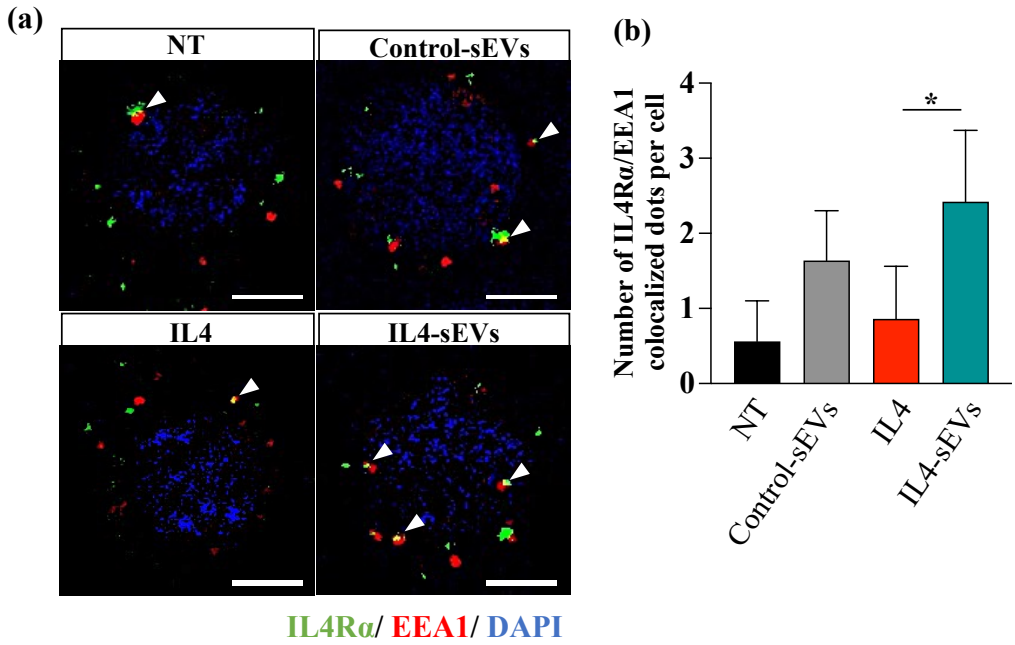

Fig. 5 Localization of IL4Rα in M1 macrophages added with IL4-sEVs.
(a) Confocal microscopy images of M1 macrophages nontreated (NT) or treated with control-sEVs, IL4, or IL4-sEVs (IL4: 60 ng/mL). Green: Alexa Fluor 488 (IL4Rα), red: Alexa Fluor 647 (early endosome), blue: DAPI (nucleus). Scale bar = 5 μm. (b) The mean number of IL4Rα/EEA1 colocalized signals per cell. At least 30 cells in each group were measured in three independent experiments. **P* < 0.05 vs IL4. The results are expressed as the mean ± standard deviation.

I-3-f IL4-sEVs ameliorated severity of collagen-induced arthritis.

To investigate the therapeutic potential of IL4-sEVs in chronic inflammatory diseases, I established CIA mice. PBS, control-sEVs, IL4, or IL4-sEVs were injected once daily into the ankle joints of CIA mice from day 27 after the onset of disease to day 36 (Fig. 6a). The intensity of arthritis was assessed in terms of the clinical score and hind paw swelling from the day of the second immunization. As shown in Fig. 6c, the CIA mice administered by IL4-sEVs daily exhibited a smaller increase in the clinical score compared to the CIA mice administered with PBS. In addition, IL4-sEVs attenuated the paw swelling in the CIA mice and were more effective than IL4 (Fig. 6d).

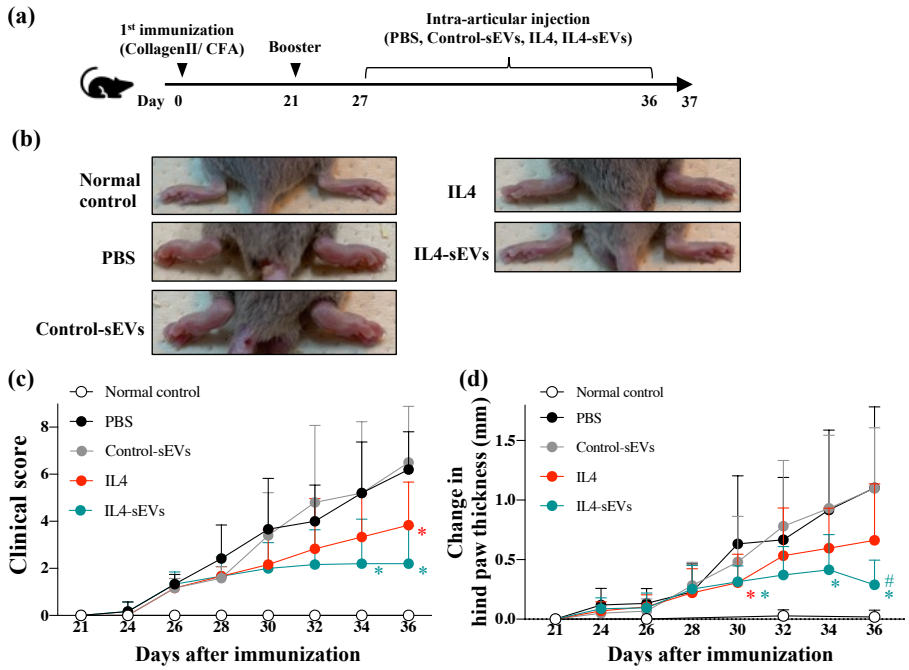

Fig. 6 Therapeutic effect of IL4-sEVs on the CIA mice.
(a) Schematic of the protocol of CIA induction and treatment. (b) Photographs of the hind paw at day 37 of normal control mice or CIA mice after the treatment by each agent (PBS, control-sEVs, IL4, or IL4-sEVs). (c) Clinical scores of the hind paws of the mice. (d) Change in hind paw thickness in mice from day 21. The results are expressed as the mean ± standard deviation (n = 3: normal control group, n = 4–6: other groups). *P < 0.05 compared to the PBS group. #P < 0.05 compared to the IL4 group.

I-3-g Joint inflammation in CIA mice was reduced by daily injection of IL4-sEVs into the joints.

I further evaluated the pathologic states of the ankle joints on day 37 (one day after the end of the treatment) by a histopathological analysis and by measuring the mRNA expression levels of pro-inflammatory cytokines in the ankle joints. Fig. 7a, b show H&E staining of ankle joints of normal control mice or CIA mice treated with PBS, control-sEVs, IL4, or IL4-sEVs. CIA-characteristic symptoms such as synovitis characterized by inflammatory cell infiltration and synovial proliferation, pannus formation, and bone destruction were identified in the joints of PBS- or control-sEV-administered mice. Although bone destruction was hardly observed in the joints of the IL4-treated mice, inflammatory infiltration, synovial proliferation, and pannus formation were observed. On the contrary, mild infiltration of inflammatory cells into the synovium was observed in the joints of the mice treated with IL4-sEVs.

The expression levels of pro-inflammatory cytokines (TNFα, IL6, IL1β, and IL12) were high in the joint tissues of the CIA mice treated with PBS. In the joint tissues of the mice administered with IL4, lower levels of pro-inflammatory cytokines were detected. However, most of these decreases were not

significant compared to the PBS-treated mice, whereas significant decreases in the pro-inflammatory cytokine expression level were observed in the tissues of the IL4-sEV-treated mice (Fig. 7c–f). Thus, the ankle joint inflammation and destruction were greatly suppressed by the daily intraarticular injection of IL4-sEVs, which shows consistent results with the clinical assessment.

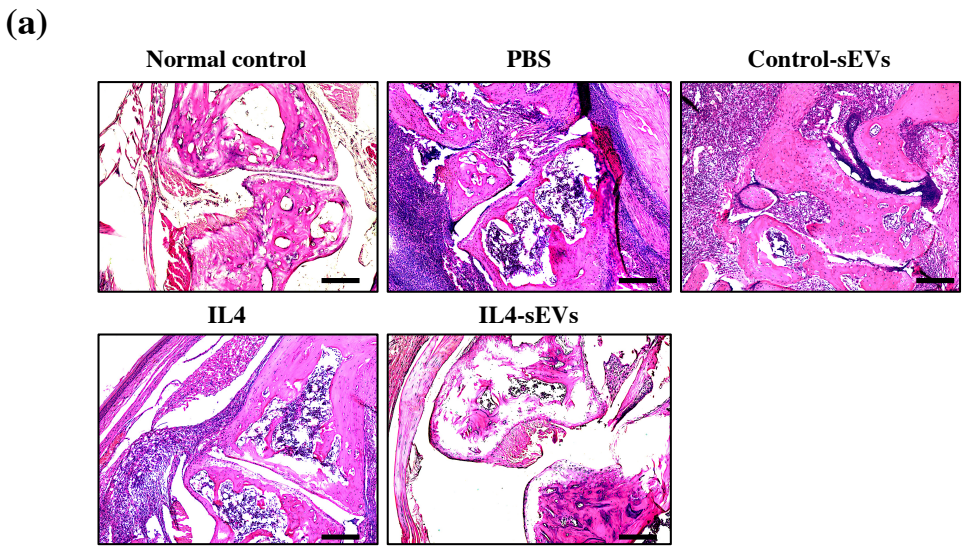

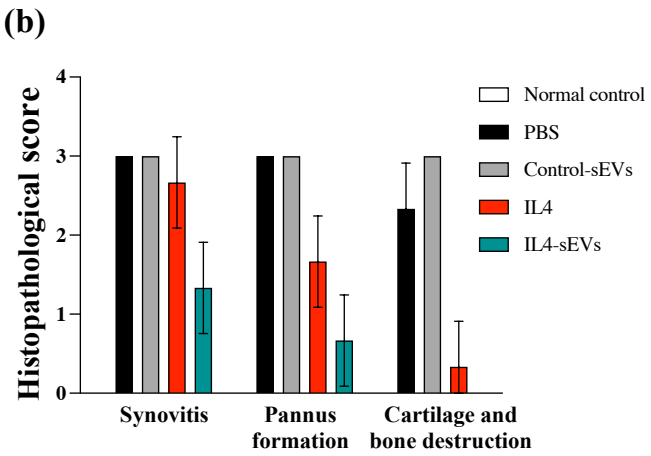

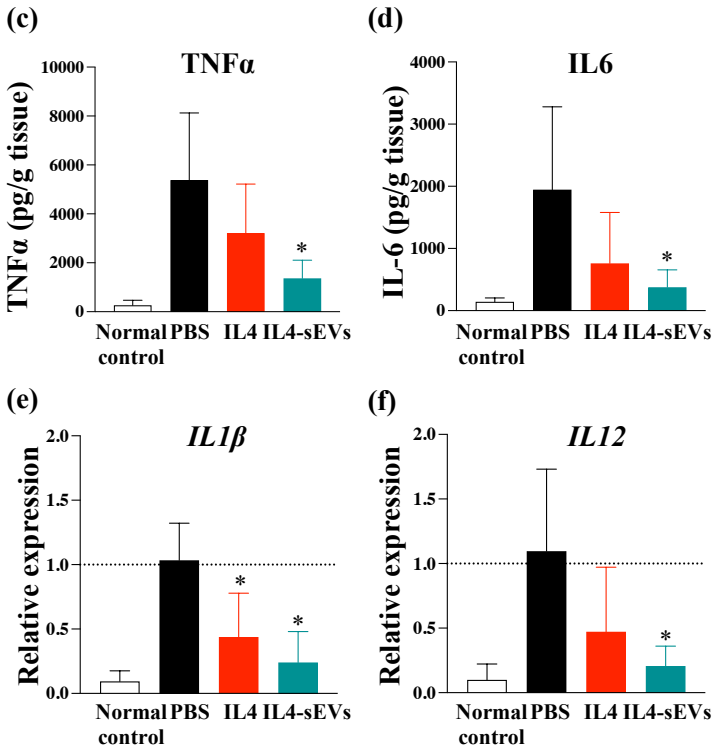

Fig. 7 Severity of joint inflammation in CIA mice after the treatment.
(a) Representative H&E-stained ankle joint tissue sections of normal control mice or CIA mice after the treatment by each agent (PBS, control-sEVs, IL4, or IL4-sEVs). Scale bar = 200 μm. (b) Histopathological score assessing synovitis, pannus formation, and cartilage and bone destruction at four grades (0–3: 0 = normal, 1 = mild, 2 = moderate, and 3 = severe). The results are expressed as the mean ± standard deviation. (c–f) TNFα, IL6, IL1β, and IL12 expressions in ankle joint tissues of the mice. The results are expressed as the mean ± standard deviation. *$P < 0.05$ compared to the PBS group.

I-3-h IL4-sEV treatment promoted the shift of synovial macrophage polarization toward the M2 phenotype.

To characterize the synovial macrophage phenotype, I assessed the M1 marker (iNOS, CXCL10, CD86) and M2 marker (Arg1, IL10, TGFβ, and CD206) expressions in ankle joint tissues. As revealed by RT-PCR, the mRNA expression levels of M1 marker genes (iNOS and CXCL10) were significantly lower in the tissues of the IL4-sEV-treated mice than in the PBS-treated mice and IL4-treated mice (Fig. 8a, b). The M2 gene (Arg1, IL10, and TGFβ) expression was largely increased in the IL4-sEV-treated ankles compared to those in the PBS-treated mice and IL4-treated mice (Fig. 8c–e). Immunohistochemical staining of CD86 (M1 marker membrane protein) and CD206 (M2 marker membrane protein) was also performed to further investigate the presence of M1 or M2 macrophages in the tissues. As shown in Fig. 8f, only a red fluorescence signal representing CD86 expression, which was not observed in the tissue of normal control mice, was observed in the PBS-treated tissues, which

shows that the joints of the CIA mice were infiltrated by M1 macrophages. In the IL4-treated ankle tissue, both red and green fluorescence signals were detected, indicating that some M1 macrophages in the joint were polarized to M2 macrophages. On the other hand, a considerably higher green fluorescence signal than the red fluorescence signal was observed in the IL4-sEVs-treated ankle tissue, which indicates that most macrophages were polarized to M2. This indicates that IL4-sEVs efficiently changed the phenotype of macrophages in the ankle joint tissues of the CIA mice. These data suggest that the anti-arthritis effects of IL4-sEVs are mediated in part by M1/M2 modulation.

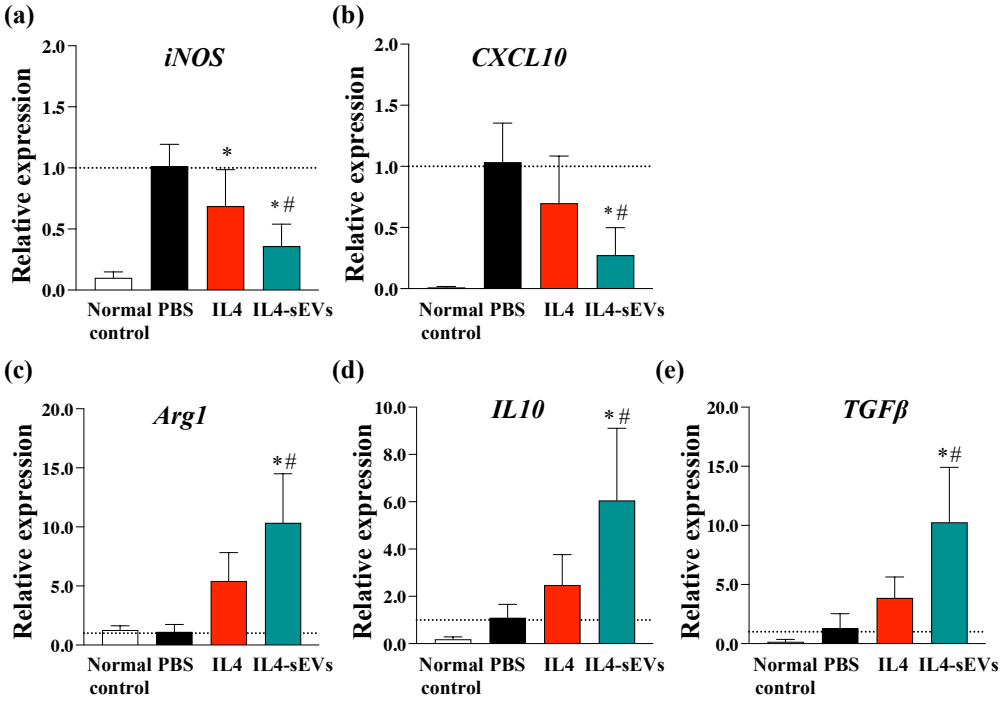

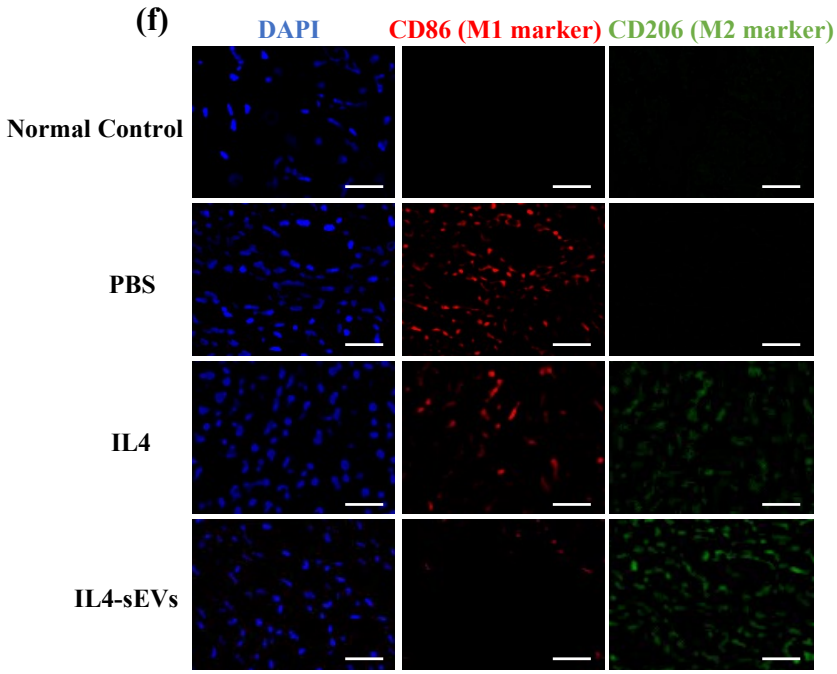

Fig. 8 Evaluation of the macrophage phenotype in hind paws of the CIA mice after the treatment. (a–e) M1 marker (iNOS and CXCL10) and M2 marker (Arg1, IL10, and TGFβ) expressions in ankle joint tissues of the mice. The results are expressed as the mean ± standard deviation. **P* < 0.05 compared to the PBS group. #*P* < 0.05 compared to the IL4 group. (f) Representative immunohistochemically stained ankle joint tissue sections of the normal control mice or CIA mice after the treatment by each agent (PBS, control-sEVs, IL4, or IL4-sEVs). Scale bar = 100 μm. Green: Alexa Fluor 488 (CD86), red: Alexa Fluor 647 (CD206), blue: DAPI (nucleus).

I-4 Discussion

Synovial macrophages are the dominant effector cells in the initiation and progression of synovitis and bone inflammation in RA, which makes them a primary target in RA therapy [36]. In this study, I proposed an anti-rheumatoid therapy based on control of M1/M2 macrophage polarization.

I selected HEK293 cells as IL4-sEV-producing cells because they can be efficiently transfected with plasmid DNA coding IL4-LA. However, given that sEVs derived from Mesenchymal stem cells (MSC), Adipose-derived stem cells (ADSC) and M2 macrophages are shown to have anti-inflammatory properties [37–39], it is expected that loading IL4 to those sEVs could enhance the anti-inflammatory effects.

IL4-sEVs exhibited similar or larger inhibitory effects on M1 macrophages and induction effects on M2 macrophages compared to those of IL4 (Fig. 3). Endocytosis inhibition of macrophages using Cytochalasin D abolished the M1-inhibitory and M2-promoting effects of both IL4 and IL4-sEVs (Fig. 4a–c), in agreement with a previous report [26], which confirmed the significance of endosomal compartments in IL4 signal transduction. It was indicated that in the case of IL4-sEVs, IL4 signaling at the endosome was triggered through endocytosis of IL4-sEVs via the recognition of their physicochemical properties by macrophages (Fig. 4d–g). The confocal images showed that sEVs fostered the IL4R localization to the early endosomes (Fig. 5), which supports the concept that the efficient endocytosis of IL4-sEVs by macrophages enhanced the IL4R internalization and subsequent IL4 signaling in the endosomal compartment, leading to the higher anti-inflammatory effects of IL4-sEVs. Interestingly, the IL4R localization to the endosomes is independent on ligand binding [25,26]. This could explain the result that nontreated macrophages exhibited almost the same number of IL4Rα/EEA1 colocalizations as that of the IL4-treated macrophages at a lower rate than that of macrophages with IL4-sEVs or control-sEVs.

The daily administration of IL4-sEVs for 10 days after the onset of the disease largely suppressed the aggravation of clinical symptoms in CIA mice (Fig. 6, 7a, b). The macrophage phenotype evaluation and pro-inflammatory cytokine profiles in the joints after the IL4-sEV treatment (Fig. 7c–f and 8) suggest that IL4-sEVs inhibited M1 activation and induced M2 activation of synovial macrophages. Thus, it was speculated that by regulating the M1/M2 status in synovial macrophages, IL4-sEVs suppressed fibroblast proliferation, pannus formation, and bone destruction in the CIA mice (Fig. 7a, b)

I believe that one of the largest benefits of this approach is that dosing can be initiated even after the onset of the disease, in which inflammatory sites are considered to be extensively infiltrated by

macrophages. In some other approaches aimed at T cell regulation or nonspecific immune suppression, therapeutic administration did not have sufficient efficacy. Therefore, dosing before the onset of the disease (preventive administration) was required [18,40]. However, the preventive administration of drugs is impractical for clinical use in RA therapy. Furthermore, while symptomatic approaches such as depletion of pro-inflammatory cytokines or inflammatory cells in the lesion do not promote tissue repair and remodeling, there is a possibility that M2 macrophages induced by IL4-sEVs promote tissue repair in joints. M2 macrophages are directly and indirectly related to wound healing [41]. M2 macrophage can ensue the recruitment and activation of Th2 immune response, which is significant for tissue repair and regeneration following joint damage in rheumatoid arthritis [42]. In addition, M2-macrophage-derived IL10, TGFβ, and BMP-2 promote osteogenesis by stimulating osteoblast differentiation [43–45]. Although the bone regeneration was not evaluated in this study, the capability of wound healing by this therapy is implied by the high expression levels of IL10 and TGFβ mRNA in the joints of the IL4-sEV-treated mice (Fig. 8d, e).

I-5 Summary of chapter 1

In this chapter, I demonstrated that IL4-loaded sEVs exhibited high anti-inflammatory effects by modulating the macrophage polarization. This indicates that sEVs enable the safe and efficient use of IL4, providing a new approach for the treatment of chronic inflammatory diseases. This is the first study developing IL4-carrying sEVs and fully utilizing their potential as both drug delivery vehicles and signal amplification vehicles.

Chapter 2

Intracellular delivery of anti-inflammatory peptides to macrophages using sEVs

II-1 Introduction

Dysregulated nuclear factor-kappa B (NF-κB) activation is related to the onset and exacerbation of various inflammatory diseases, such as metabolic disorders, autoimmune diseases, and cancer [46–48] Especially excessive activation of NF-κB in macrophages contributes to those inflammatory diseases mainly through the enhanced expression of proinflammatory mediators [49]. Therefore, inhibiting NF-κB activation in macrophages can serve as a strategy for the treatment of various inflammatory diseases.

The NEMO binding domain (NBD) peptide is an NF-κB inhibitor that specifically binds to NEMO, one of the components of the IκB kinase (IKK) complex, and blocks the interaction between NEMO and IKKβ [50,51]. The IKK complex is composed of two protein kinase subunits, IKKα and IKKβ, and a regulatory component, NEMO, and NF-κB is mostly activated through IKKβ-mediated phosphorylation and degradation of IκB proteins [52–55]. Therefore, the suppression of IKK activation by NBD peptide via blocking the interaction between NEMO and IKKβ, inhibits NF-κB activation and the subsequent transcription of various proinflammatory genes [56–58]. However, as NEMO is located in the cytosol, the NBD peptide has to be stably internalized into the cells to exert its NF-κB inhibitory effects. Thus, a delivery system is needed to overcome the membrane impermeability and low stability of NBD peptides.

Owing to their intrinsic properties as endogenous delivery carriers, and macrophage-targeting properties, sEVs were considered to be a promising delivery carrier of NBD peptides into macrophages [59–61]. Previous report suggested that cargos which were internally-loaded to sEVs were delivered into the cytosol more efficiently than those externally loaded on sEVs [62].

In this chapter, I developed a method to load the NBD peptide into sEVs by constructing plasmids encoding a fusion protein of Gag—that binds to the phosphatidylinositol-4,5- bisphosphate [PI(4,5)P2] in the inner membrane of sEVs [63]—and NBD peptides. As the NBD peptide demonstrates biological activity by binding to NEMO [50], and the interaction efficiency could be determined by the number of NBD molecules, I designed three types of fusion proteins containing one, three, or six repeats of NBD peptides. sEVs were isolated from HEK293 cells transfected with the plasmid constructs described above. After confirming the internal loading of the fusion proteins in the isolated sEVs, I investigated the inhibitory effects of the NBD peptide-containing sEVs (nNBD-sEVs) on NF-κB activation and the subsequent production of proinflammatory mediators in LPS-stimulated macrophages.

II-2 Materials & Methods

Cell culture

The murine macrophage cell line RAW264.7 and Human Embryonic Kidney cells 293 (HEK293) were obtained and cultured as described in Chapter 1.

Construction of plasmids

The gene sequence encoding Gag was obtained, as described in the previous report [63]. First, C-terminal FLAG-tagged Gag sequence was constructed using a two-step PCR. Then, the Gag- FLAG encoding sequence was fused with the NBD sequence, three repeats of the NBD sequence, and six repeats of the NBD sequence using a two-step PCR, to obtain Gag-FLAG-1NBD, Gag- FLAG-3NBD, and Gag-FLAG-6NBD, respectively. Sequences of the primers used for cloning are available upon request. To construct the pCMV constructs encoding the corresponding fusion proteins, the cDNAs encoding the fusion proteins were cloned into the EcoRI/NotI site of the pcDNA3.1 vector (Thermo Fisher Scientific, Inc., USA), and those encoding the Gag-FLAG- 3NBD fusion protein were cloned into the EcoRI/XhoI site of the pcDNA3.1 vector (Thermo Fisher Scientific).

Isolation of sEVs

The HEK293 cells (4.0×10^6 cells) were transfected with the constructs encoding the Gag- FLAG-nNBD fusion proteins using PEI Max (Polysciences, Inc., USA), as described previously [32]. sEVs were isolated from culture supernatants of non-transfected and transfected cells according to the method described in chapter 1. The amount of isolated sEVs was estimated by measuring the protein concentration using the Bradford assay.

Preparation of cell lysates

All cell lysates were prepared via multiple rounds of freezing and thawing followed by centrifugation at 15000 × g for 15 min. Additionally for the analysis of NF-κB pathway-related proteins, phosphatase inhibitor cocktail (Nacalai Tesque Inc., Japan) was added. Protein concentration was measured using the Bradford assay.

Transmission electron microscopy (TEM) observation

The sEV samples were observed by TEM according to the method described in chapter 1.

Measuring of zeta potential

Zeta potential of sEVs was measured according to the method described in chapter 1.

Flow cytometry

The sEVs were stained using the PKH67 green fluorescent cell linker kit purchased from Sigma-Aldrich, as described previously [32]. Briefly, sEVs were mixed with 2 μM PKH67 dye prepared in Diluent C and incubated for 5 min at 25 °C. The staining reaction was stopped by addition of 5% bovine serum albumin prepared in PBS, and the samples were ultracentrifuged at 100000 × g for 1 h to remove the free PKH67 dye. The pellets were resuspended in PBS and PKH67-labeled sEVs were prepared. RAW264.7 cells were cultured overnight in a 96-well plate and were replaced with Opti-MEM (Thermo Fisher Scientific). The PKH67-labeled control-sEVs and nNBD-sEVs (n=1, 3, 6) were added to the cells at a concentration of 10 μg/mL, followed by incubation for 4 h at 37 °C. Next, the cells were washed thrice with PBS, and were then suspended in the same. The cellular uptake of PKH67-labeled sEVs was determined using the Gallios Flow Cytometer (Beckman Coulter, USA) according to the manufacturer's instructions. Data were analyzed using the Kaluza software (Beckman Coulter, USA) to determine the mean fluorescence intensity (MFI).

Western blotting

HSP70, CD81, Alix and Calnexin of sEV samples and HEK293 cells, and iNOS and GAPDH of RAW264.7 cells were detected according to the method described in previous chapter. FLAG of sEV samples was detected using mouse anti-FLAG M2 monoclonal antibody (1:10000; Sigma-Aldrich, USA). IKKβ, Phospho-IKKα/β (Ser176/180), IκBα, Phospho-IκBα (Ser32), NF-κB p65 and Phospho-NF-κB p65 (Ser536) of RAW264.7 cells were detected using rabbit anti-IKKβ antibody (1:1000; Cell Signaling Technology), rabbit anti-Phospho-IKKα/β (Ser176/180) antibody (1:1000; Cell Signaling Technology), mouse anti-IκBα antibody (1:1000; Cell Signaling Technology), rabbit anti-Phospho-IκBα (Ser32) antibody (1:1000; Cell Signaling Technology), rabbit anti-NF-κB p65 antibody (1:1000; Cell Signaling Technology), and rabbit anti-Phospho-NF-κB p65 (Ser536) antibody (1:1000; Cell Signaling Technology).

NF-κB reporter assay

RAW264.7 cells seeded in a 100 mm culture dish at a density of 5.0 × 10^5 cells/mL were co-transfected with pNF-κB-Luc (Mercury Pathway Profiling Luciferase system 1; BD Biosciences Clontech, USA) and phRL-TK vector encoding Renilla luciferase (Promega, USA; internal control) using Lipofectamine 2000 (Thermo Fisher Scientific) according to the manufacturer's protocol. After a 4-h incubation period, the cells were seeded into a 96-well plate at a density of 2.0 × 105 cells/mL and incubated overnight at 37 °C. The culture medium was replaced with Opti- MEM and the cells were treated with control-sEVs, 50μM curcumin (dissolved in ethanol), or nNBD-sEVs (n=1, 3, 6) for 4 h, followed by stimulation with 0.1–100 ng/mL of LPS (Sigma- Aldrich). After a 5-h incubation period, the cells were washed and lysed with lysis buffer supplied along with the luciferase assay kit (Piccagene Dual, Toyo Ink, Japan). The luciferase activity was measured using the abovementioned kit (Piccagene Dual), and chemiluminescence was measured using a luminometer (Lumat LB9507; EG and GBerthold, Germany). The fold induction in luciferase activity was calculated by normalizing the firefly luciferase activity to the Renilla luciferase activity.

Assessment of the expression of NF-κB pathway-related proteins

RAW264.7 cells were seeded into a 12-well plate at a density of 2.0 × 10^5 cells/mL and incubated overnight at 37 °C. The medium was replaced with Opti-MEM, and the cells were treated with control-sEVs, curcumin (dissolved in ethanol) (Sigma-Aldrich), 1NBD-sEVs, or 6NBD-sEVs for 4 h. Next, the cells were stimulated with LPS (10 ng/mL) for 1 h, after which the cell lysates were prepared as mentioned above.

Quantification of cytokine secretion

RAW264.7 cells (2.0 × 10^5 cells/mL) were incubated in a 96-well plate overnight at 37 °C . The medium was replaced with Opti-MEM, and cells were pretreated with control-sEVs, curcumin (dissolved in ethanol), 1NBD-sEVs, and 6NBD-sEVs for 30 min, followed by stimulation with LPS (10 ng/mL). After a 24-h incubation, the supernatants were collected and the concentration of TNFα was measured using mouse TNFα enzyme-linked immunosorbent assay (ELISA) OptEIA sets (Pharmingen, USA) according to the manufacturer's instructions.

mRNA extraction and quantitative real-time polymerase chain reaction (qRT-PCR)

RAW264.7 cells were seeded into a 48-well plate at a density of 2.0×10^5 cells/mL and incubated overnight. The medium was replaced with Opti-MEM, and cells were pretreated with control- sEVs, 50μM curcumin (dissolved in ethanol), 1NBD-sEVs, and 6NBD-sEVs for 4 h. Cells were then stimulated with LPS (10 ng/mL) for 12 h, following which total RNA was extracted as described in previous chapter. qRT-PCR was conducted according to the method described in chapter 1 using the primers of GAPDH, iNOS and CXCL10.

Measurement of iNOS expression and NO production

RAW264.7 cells (2.0×10^5 cells/mL) were incubated overnight in a 48-well plate. The medium was replaced with Opti-MEM, and the cells were pretreated with the control-sEVs, 50μM curcumin (dissolved in ethanol), 1NBD-sEVs, and 6NBD-sEVs for 4 h. Next, the cells were stimulated with LPS (10 ng/mL) for 12 h. For evaluating iNOS expression, the cell lysates were prepared as described above. For the measurement of NO production, the supernatants were collected and the NO concentration was determined using the Griess Reagent Kit (Biotium, USA) according to manufacturer's instructions. Samples were analyzed using a plate reader (Multiskan, Thermo Fisher Scientific Inc.) by measuring the absorbance (OD570/OD620).

Statistical analysis

Statistical differences were evaluated using a one-way analysis of variance (ANOVA), followed by the Tukey–Kramer multiple comparison test; $p<0.05$ was considered statistically significant.

II-3 Results

II-3-a Three plasmids were constructed and NBD-containing sEVs (nNBD-sEVs) were isolated.

Plasmids encoding the Gag-FLAG-1NBD, Gag-FLAG-3NBD, and Gag-FLAG-6NBD were constructed (Fig. 9a). Western blotting for the FLAG tag indicated that all the fusion proteins were loaded to the sEVs. As the FLAG signals were detected even after the protease K treatment erased the CD81-derived signal (Fig. 9c), it was confirmed that all the NBD fusion proteins were loaded into the internal space of sEVs.

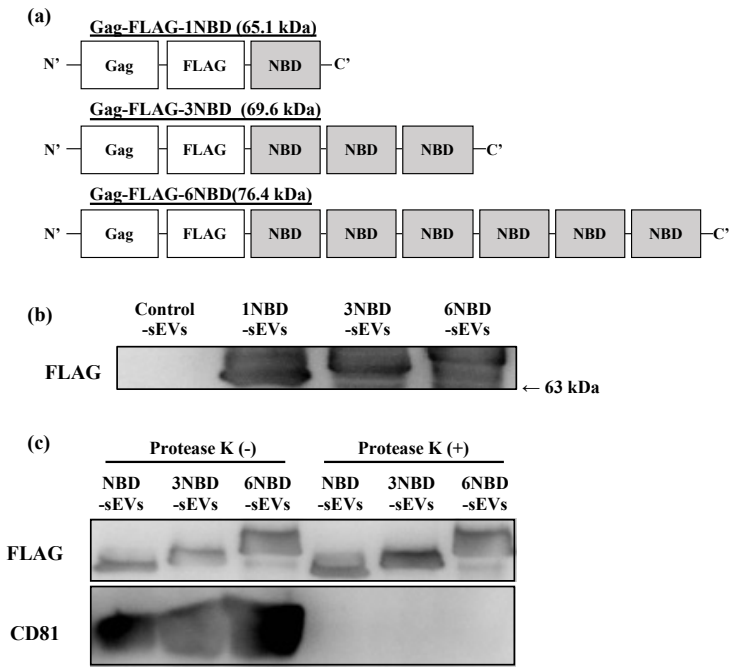

Fig. 9 Plasmid construction and confirmation of nNBD-sEV (n=1, 3, 6) isolation from HEK293 cells.
(a) Plasmids encoding Gag-FLAG-1NBD, Gag-FLAG-3NBD, and Gag-FLAG-6NBD. (b) Western blot analysis of control-sEVs and nNBD-sEVs (n=1, 3, 6) using the FLAG antibody. The arrow indicate positions of the bands representing molecular weight markers. (c) Western blotting for control-sEVs and nNBD-sEVs (n=1, 3, 6) treated with protease K/untreated, detected using the FLAG or CD81 antibodies.

II-3-b The physicochemical properties of sEVs were not altered significantly upon NBD-loading.

Western blotting for sEV marker proteins, HSP70, AlIX, and CD81, confirmed the successful isolation of sEVs from the culture medium of non-transfected HEK293 cells and HEK293 cells transfected with the three plasmid constructs (Fig. 10a). Calnexin, an endoplasmic reticulum marker, was undetected in all sEVs, confirming the negligible contamination from cell-derived debris in the collected samples (Fig. 10a). To evaluate the physicochemical properties of sEVs, these were subjected to TEM observation and zeta potential measurement. The TEM images revealed that all sEVs had a similar morphology and size distribution profile (Fig. 10b). Zeta potential values of all collected sEV samples were comparable (Fig. 10c). These results suggest that the loading of fusion proteins did not significantly alter the physicochemical properties of sEVs.

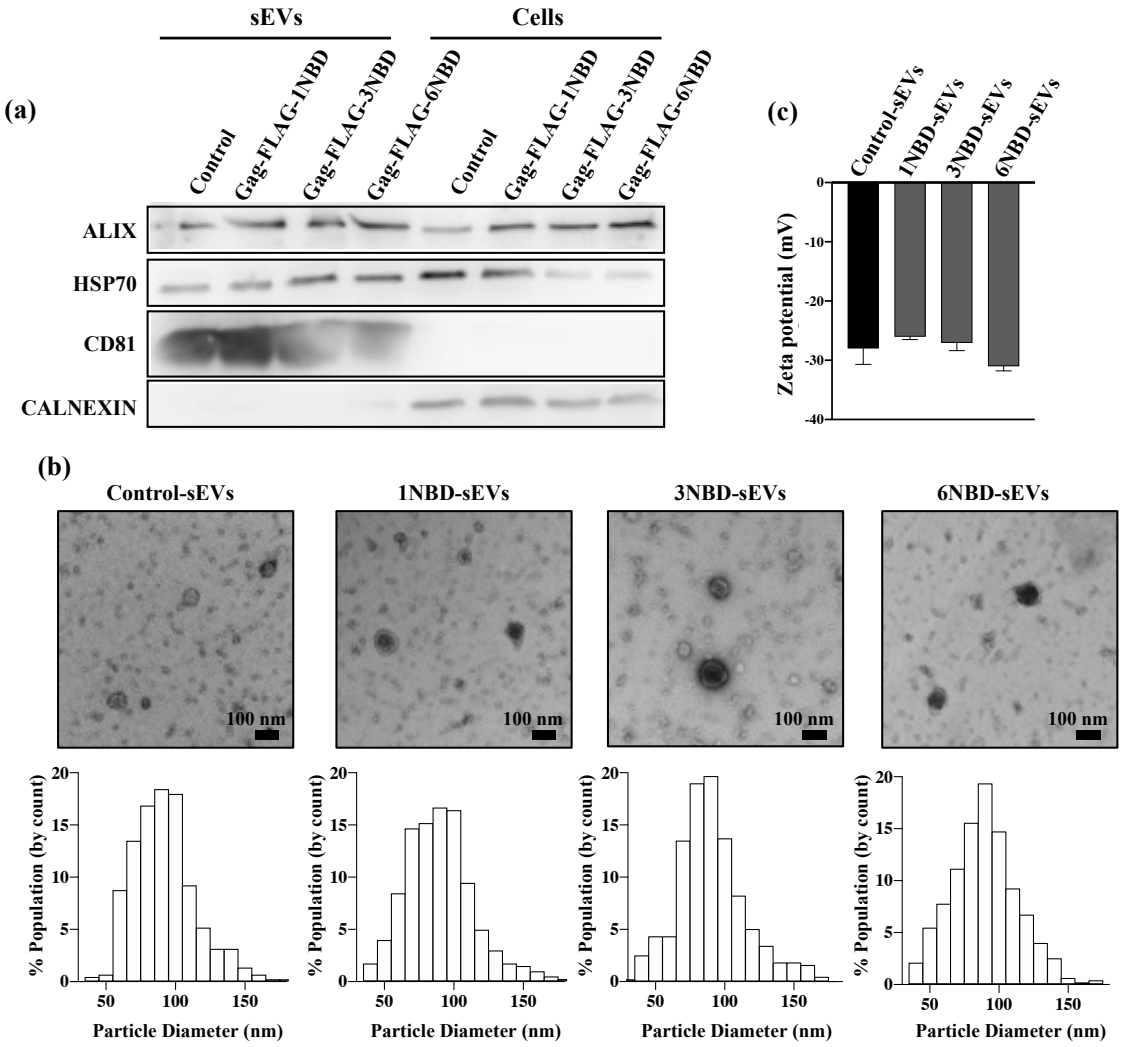

Fig. 10 Identification of NBD-loaded sEVs.
(a) Western blotting for HSP70, CD81, ALI X, and Calnexin in control-sEVs, nNBD-sEVs (n=1, 3, 6), and HEK293 cell lysates (5 μg of protein). (b) Transmission electron microscopy (TEM) images (Scale bar=100 nm) and histograms of particle size distribution of control-sEVs and nNBD-sEVs (n=1, 3, 6). (c) Zeta potential of control-sEVs and nNBD-sEVs (n=1, 3, 6). Results are expressed as the mean ± standard deviation (n=3).

II-3-c Loading of fusion proteins into the sEVs did not affect the sEV uptake efficiency in RAW264.7 murine macrophages.

Subsequently, the cellular uptake of sEVs by the RAW264.7 cells was evaluated using flow cytometry. No significant differences were observed in the MFI of cells treated with control-sEVs and nNBD-sEVs (n=1, 3, 6) (Fig. 11). This indicates that loading of fusion proteins into sEVs had a limited effect on the sEV uptake efficiency of macrophages.

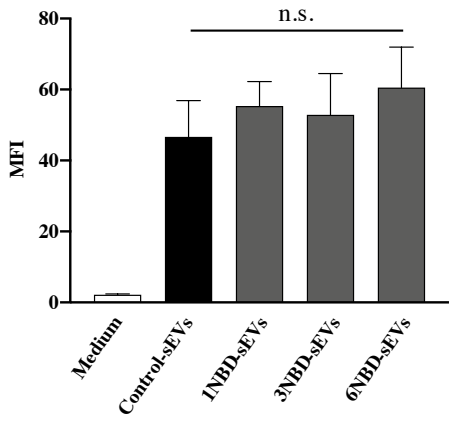

Fig. 11 Cellular uptake of sEVs by RAW264.7 murine macrophages.
RAW264.7 murine macrophages were treated with PKH67-labeled control-sEVs and nNBD-sEVs (n=1, 3, 6). After a 4-h incubation period, the mean fluorescence intensity (MFI) of the cells was measured using fluorescence-activated cell sorting to evaluate the cellular uptake of sEVs. Results are expressed as the mean ± standard deviation (n = 3). n.s., not significantly different.

II-3-d 6NBD-sEVs blocked the nuclear translocation of LPS-induced NF-κB in RAW264.7 cells.

Next, to investigate whether the nNBD-sEVs (n=1, 3, 6) exerted inhibitory effects with respect to NF-κB activation we used reporter assays after confirming LPS-induced dose-dependent increase in reporter gene expression in RAW264.7 cells (Fig. 12a). The results revealed that the fold induction in RAW264.7 cells pretreated with 6NBD-sEVs was significantly lower than that in non-treatment (NT) cells (Fig. 12b). Conversely, there were no significant differences between the fold induction in cells pretreated with 1NBD-sEVs or 3NBD-sEVs and that in NT cells. These results suggest that the 6NBD-sEVs had the ability to inhibit the translocation of NF-κB to the nucleus; however, the 1NBD-sEVs and 3NBD-sEVs had limited ability to inhibit NF-κB activation. As it was confirmed that both 1NBD-sEVs and 3NBD-sEVs exerted limited inhibitory effects on NF-κB activation, the 3NBD-sEVs were excluded from the following experiments.

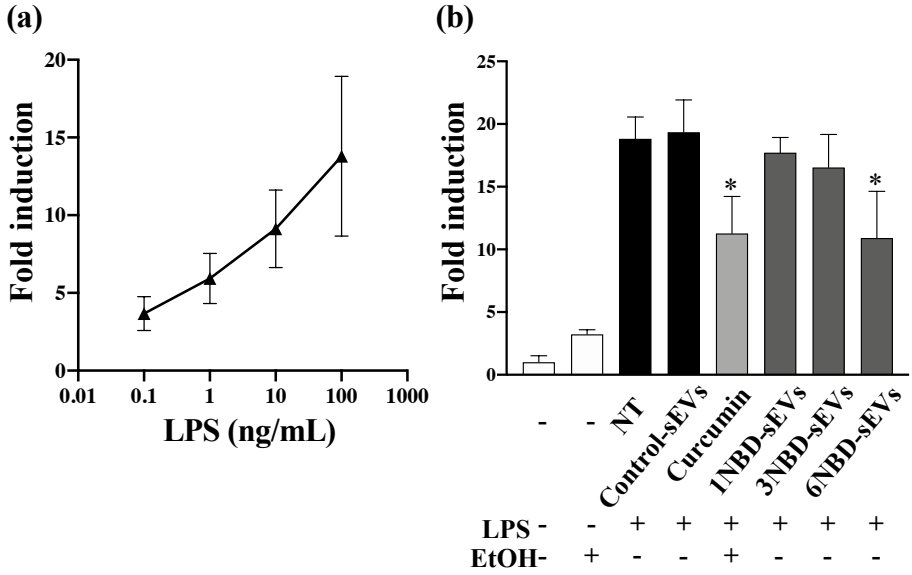

Fig. 12 NF-κB reporter assay in RAW264.7 murine macrophages.
(a) The fold induction in NF-κB reporter activity in RAW264.7 cells stimulated with the indicated concentrations of LPS. (b) NF-κB reporter assay in RAW264.7 cells pretreated with control-sEVs, curcumin, or nNBD-sEVs (n=1, 3, 6), and subsequently stimulated with LPS. Results are expressed as the mean ± standard deviation (n=4). *P<0.05 compared to the non-treatment (NT) group.

II-3-e LPS-induced phosphorylation of IKKα/β, IκBα, and NF-κB p65 proteins in RAW264.7 cells was inhibited by the 6NBD-sEVs.

The mechanism underlying the inhibitory action of 6NBD-sEVs on the NF-κB signaling pathway was investigated. As it has been reported that the NBD peptide binds to NEMO and inhibits the phosphorylation of IKKα/β [50,58,64], we performed western blotting to assess the phosphorylation status of proteins that are a part of the protein complex. The analysis revealed that compared to that in cells of the NT group, the phosphorylation of IKKα/β proteins in LPS-stimulated RAW264.7 cells reduced after pretreatment with curcumin or 6NBD-sEVs, whereas pretreatment with control-sEVs or 1NBD-sEVs did not induce the same effect (Fig. 13). Subsequently, the phosphorylation status of IκBα and NF-κB p65 was also evaluated. The phosphorylation levels of these two proteins were also reduced upon pretreatment with curcumin or 6NBD-sEVs (Fig. 13). These results indicate that the 6NBD-sEVs inhibit NF-κB activation *via* the inhibition of its kinase activity and *via* the inhibition of IKKα/β phosphorylation.

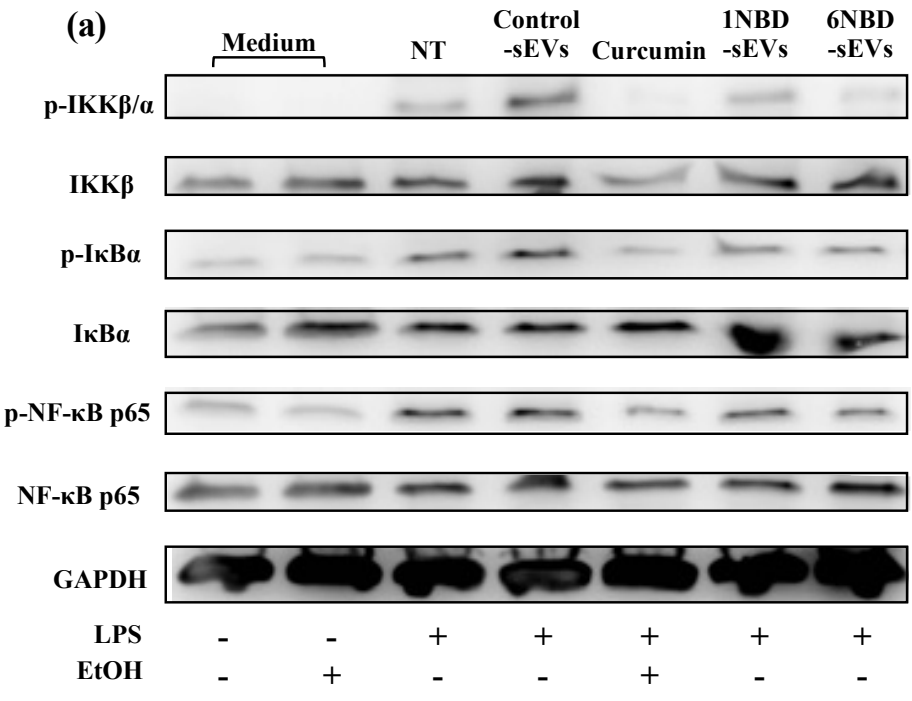

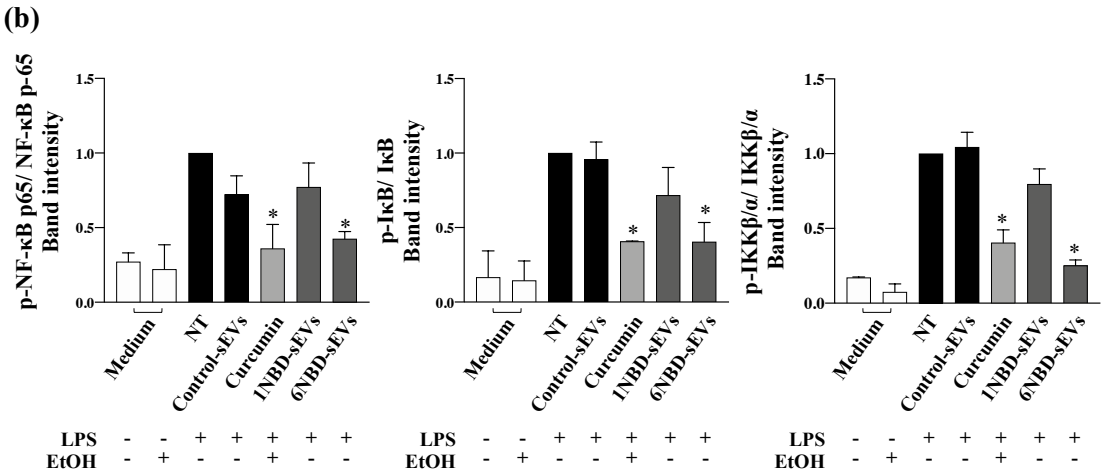

Fig. 13 Western blotting for evaluating the phosphorylation status of proteins involved in the NF-κB pathway.

(a) Western blot analysis of cell lysates (15 μg of protein) that were treated with control-sEVs, curcumin, 1NBD-sEVs, or 6NBD-sEVs, followed by LPS stimulation, detected using antibodies against IKKα/β, p-IKKα/β, IκBα, p-IκBα, NF-κB p65, p-NF- κB p65, and GAPDH. Representative blots of three independent experiments are shown. (b) The ratio of the band intensity of phosphorylated protein to that of the total protein, after normalized by the band intensity of the correspondent GAPDH. Data are presented as the mean ± standard deviation in fold change over NT group, obtained from three independent experiments. *$p<0.05$ vs NT group.

II-3-f 6NBD-sEVs suppressed NF-κB-dependent cytokine and chemokine expression in RAW264.7 cells.

I further investigated whether 6NBD-sEVs exerted inhibitory effects on the expression of NF-κB-induced proinflammatory cytokines (TNF-α) and chemokines (CXCL10). ELISA revealed that the levels of TNF-α secreted by LPS-stimulated RAW264.7 cells pretreated with 6NBD-sEVs were significantly lower than those secreted by NT cells, and that this was a concentration-dependent effect (Fig. 14a). Conversely, pretreatment with control-sEVs or 1NBD-sEVs exerted limited inhibitory effects. Additionally, the expression of *CXCL10* mRNA reduced in response to pretreatment with 6NBD-sEVs (Fig. 14b). These results suggest that the 6NBD-sEVs inhibited cytokine and chemokine expression in LPS-stimulated RAW264.7 cells by downregulating the NF-κB activity.

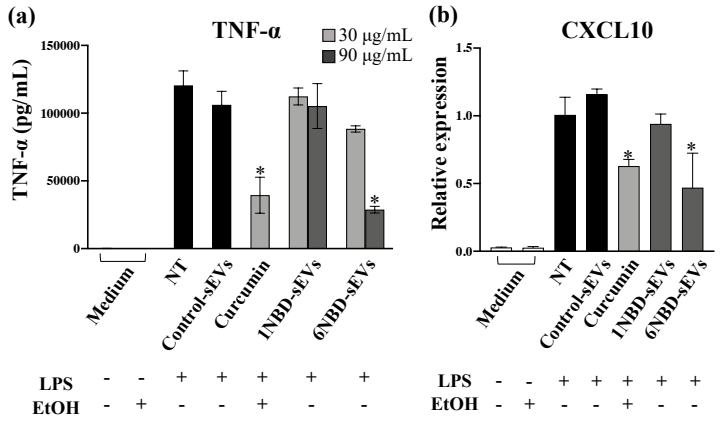

Fig. 14 Inflammatory cytokine (TNF-α) and chemokine (CXCL10) expression in RAW264.7 cells.
(a) TNF-α levels in the supernatant of RAW264.7 cells stimulated with LPS in the presence of control-sEVs, curcumin, 1NBD-sEVs, or 6NBD-sEVs using ELISA. (b) *CXCL10* mRNA expression in LPS-stimulated RAW264.7 cells pretreated with control-sEVs, curcumin, 1NBD-sEVs, or 6NBD-sEVs using RT-PCR. Results are expressed as the mean ± standard deviation (n=4). *P<0.05 compared to the NT group.

II-3-g Expression of the NF-κB-regulated inflammatory genes was inhibited by the 6NBD-sEVs.

In addition to TNF-α and *CXCL10*, the inhibitory effect of 6NBD-sEVs on *iNOS*—another inflammatory gene—was evaluated. The expression of *iNOS* at mRNA and protein levels in LPS-stimulated RAW264.7 cells pretreated with 6NBD-sEVs reduced significantly compared to that in NT cells (Fig. 15a and 15b). Furthermore, the concentration of NO, an inflammatory mediator synthesized by iNOS, was reduced in response to 6NBD-sEV exposure, which corresponds to the results regarding *iNOS* expression (Fig. 15c).

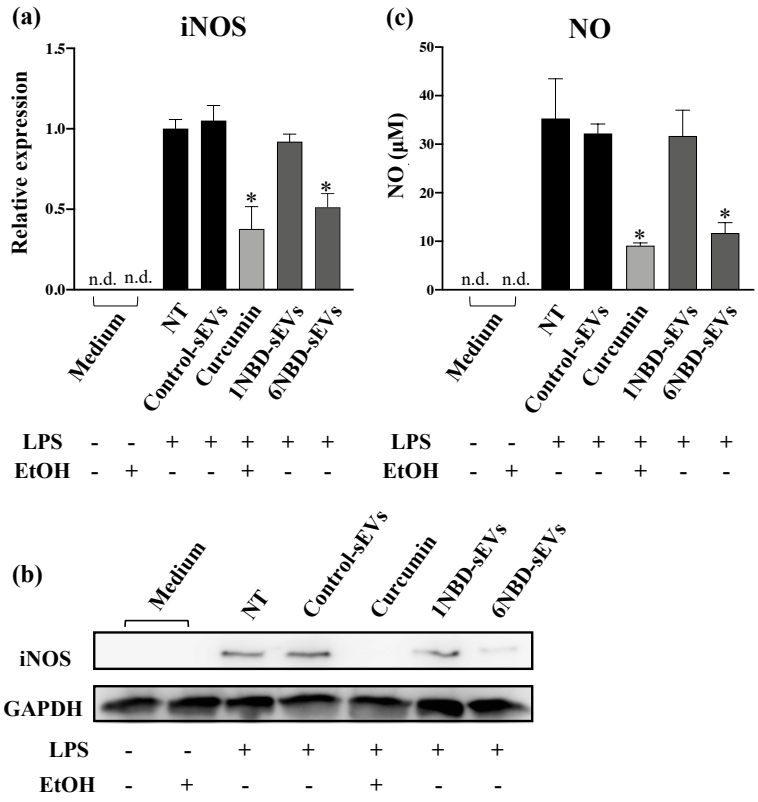

Fig. 15 Expression of iNOS and subsequent NO production in RAW264.7 cells.
(a) Evaluation of iNOS mRNA expression in LPS-stimulated RAW264.7 cells pretreated with control-sEVs, curcumin, 1NBD-sEVs, or 6NBD-sEVs using RT-PCR. Results are expressed as the mean ± standard deviation (n=4). *P<0.05 compared to the NT group. (b) Western blotting for iNOS in LPS-stimulated RAW264.7 cells pretreated with control-sEVs, curcumin, 1NBD-sEVs, or 6NBD-sEVs. In each lane, 15 μg protein of cell lysates were loaded. (c) NO concentration in LPS-stimulated RAW264.7 cells pretreated with control-sEVs, curcumin, 1NBD-sEVs, or 6NBD-sEVs. Results are expressed as the mean ± standard deviation (n = 4). *P<0.05 compared to the NT group.

II-3-h Anti-inflammatory effects of 6NBD-sEVs were obtained from sEV-mediated delivery of NBD peptides.

Finally, I investigated whether NBD peptide uptake by macrophages was truly sEV-dependent. I conducted NF-κB reporter assay and iNOS western blotting with lysed nNBD-sEVs. The result of NF-κB reporter assay revealed that there were no significant differences between the fold induction of luciferase activity in RAW264.7 cells preincubated with detergent-treated 6NBD-sEVs and that in non-treatment cells, although the fold induction was significantly decreased by pretreatment with 6NBD-sEVs without detergent (Fig. 16a).Then, it was also revealed that detergent-treated 6NBD-sEVs hardly decreased iNOS protein expression in LPS-stimulated RAW264.7 cells (Fig. 16b). These results suggest that the transfer of NBD peptides to the cytosol was occurred through sEV uptake by macrophages, and the anti-inflammatory effects were obtained by sEV-mediated efficient delivery of NBD peptides.

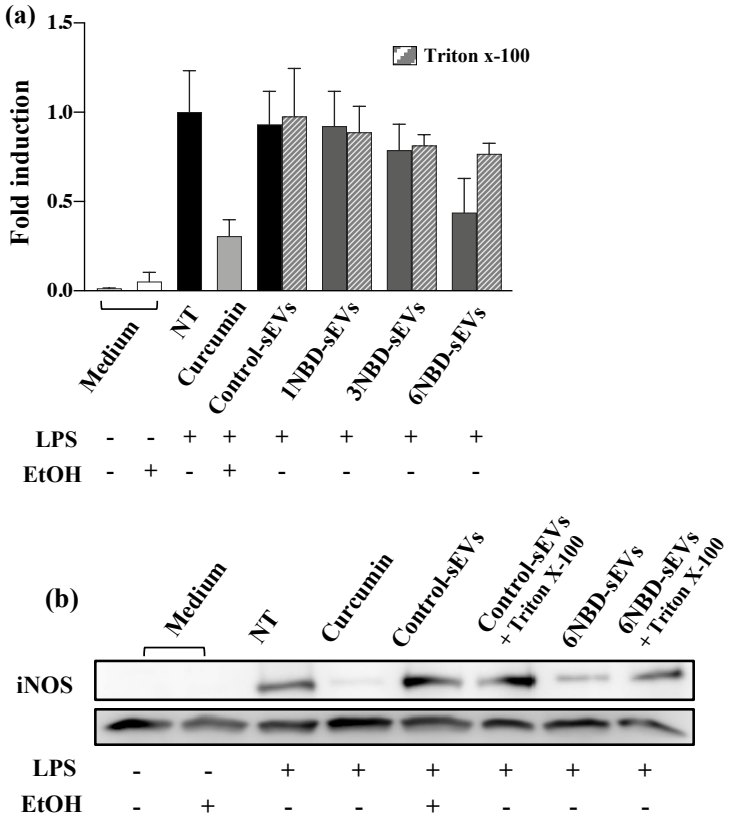

Fig. 16 Expression of NF-κB reporter gene and iNOS in RAW264.7 cells pretreated with lysed nNBD-sEVs. (a) NF-κB reporter assay in RAW264.7 cells pretreated with control-sEVs, nNBD-sEVs (n=1, 3, 6) with or without detergent-treatment, or curcumin, and subsequently stimulated with LPS. Results are expressed as the mean ± standard deviation (n=4). *P<0.05 compared to the non-treatment (NT) group. (b) Western blotting for iNOS in LPS-stimulated RAW264.7 cells pretreated with control-sEVs, 6NBD-sEVs with or without detergent-treatment, or curcumin. In each lane, 15 μg protein of cell lysates were loaded.

II-4 Discussion

The NBD peptide has been reported to be a potent NF-κB inhibitor [56–58]. To maximize the NF-κB inhibitory effects of the NBD peptide, it is necessary to deliver the peptide into the target cells. Herein, I developed a method for delivering the NBD peptides efficiently into inflammatory macrophages using sEVs. Considering the mechanism underlying the action of NBD peptide, which involves binding to NEMO, it was considered that the extent of anti-inflammatory effect might be affected by the quantity of loaded peptides. Therefore, I constructed fusion proteins containing several NBD peptides, and optimized the quantity of NBD peptides loaded into the sEVs.

In western blotting, the FLAG tag of nNBD-sEVs was retained after protease K treatment, suggesting that nNBD-sEVs can avoid degradation before and after their uptake by macrophages *via* endocytosis [27,61].

As mentioned earlier, sEV uptake by macrophages mostly occurs through the recognition of PS-

derived negative charges on the membrane surface of sEVs. In this study, nNBD-sEVs were taken up by macrophages as efficiently as control-sEVs (Fig. 11), reflecting the result that nNBD- and control-sEVs had a similar negative charge (Fig. 10).

Subsequently, the biological activity of nNBD-sEVs was examined using the reporter assay (Fig. 12). Only the 6NBD-sEVs significantly inhibited LPS-induced NF-κB activation in macrophages. The result indicates that the interaction between the NBD peptide internalized into the cytosol and NEMO was enhanced upon increasing the repeat number of NBD loaded into sEVs, and that the binding number of NBD peptide in 6NBD-sEVs with NEMO reached a sufficient number to demonstrate NF-κB inhibitory effects. Western blot analysis of the phosphorylation status of NF-κB pathway-related proteins also indicate that the NBD peptides in sEVs bound to NEMO in the cytosol, resulting in the inhibition of IKKα/β phosphorylation and subsequent downstream signaling (Fig. 13).

The 6NBD-sEVs inhibited the secretion and expression of TNF-α, *CXCL10*, *iNOS*, and NO, possibly through NF-κB inhibition (Fig. 14, Fig. 15). The inhibition of multiple proinflammatory mediators by the NBD peptide confirms that NF-κB is an important target molecule in inflammation.

The result that free Gag-NBD fusion proteins exposed after sEV membrane disruption did not exhibit anti-inflammatory effects (Fig. 16) verifies that the anti-inflammatory effects observed in the current study were obtained sEV-mediated NBD peptide delivery to macrophages. This time, we selected the NBD peptide as a therapeutic peptide, and sEVs can be applied to macrophage delivery of other peptides, such as GSK3 inhibitor peptide [65,66], JNK and p38 MAPK pathway inhibitor peptide [67,68], and HSP90 inhibitor peptide [69,70].

II-5 Summary of chapter 2

In this chapter, I demonstrated that sEVs successfully delivered bioactive peptides into macrophage cytoplasm suggesting the potential of sEVs as an intracellular delivery carrier. It was found that there was positive correlation between the loading number of peptides in sEVs and the magnitude of anti-inflammatory effect.

Chapter 3

Development of lEV-based, tumor associated macrophage (TAM)-targeted anti-cancer therapy

III-1 Summary of chapter 3

In the tumor microenvironment (TME), it has been reported that tumor-associated macrophages (TAMs), displaying M2-like property [1], play a major role to suppress immune cell response and create the pro-tumoral environment [73,74]. This immunosuppression by M2-TAMs contributes to the resistance against immune checkpoint inhibitors [75,76]. Considering this, it was assumed that therapeutics that can alter TAMs from immunosuppressive M2 phenotype to immunostimulatory M1 phenotype would assist the anti-cancer effect of immune checkpoint inhibitors by enhancing the immune response against cancer. Protein kinase A (PKA) and signal transducer and activator of transcription 3 (STAT3) are overexpressed in M2-TAMs. They increase the expression of immunosuppressive genes and decrease the expression of immunostimulatory genes in TAMs [77,78]. There are several peptides that efficiently inhibit PKA or STAT3 signaling, however, since both PKA and STAT3 are localized in the cytoplasm, those peptides require delivery systems [79,80].

In chapter 2, I found that the amount of cargoes loaded inside of sEVs was an important factor to obtain pharmacological effect. Based on this finding, I considered that a method for loading huge number of therapeutic peptides/proteins into EVs can enhance their potency as a drug delivery carrier. Thus, in this chapter, I initially attempted to establish a method for loading therapeutic peptides/proteins into lEVs, which have larger inner space for drug loading than sEVs. By using Gag protein, which binds to EV inner membrane, and two proteins, which form a stable complex, efficient peptide/protein loading into lEVs was achieved. Then, I developed lEVs multiply loaded with PKA inhibitor peptides (PKI) or STAT3 inhibitor peptides (STAT3i) by using the developed method. The ability of peptide-loaded lEVs to regulate TAM polarization, and to enhance anti-cancer effect of anti-PD-1 antibody on breast cancer mice was evaluated.

Conclusion

Dysregulation of macrophage function is associated with the onset and progress of inflammatory diseases, metabolic diseases, cancer, and so on. Therefore, controlling macrophage activation can be a promising treatment for these various diseases. EVs are membrane vesicles secreted by wide variety of cells, which recently have been researched for the clinical use as biomarkers, therapeutics and DDS carriers. Since systemically administered EVs are mostly taken up by macrophages, I considered that EVs could be applied for the development of macrophage-targeted therapeutics. Moreover, bioactive molecules such as peptides and proteins can be simply loaded to EVs by using genetic engineering, which was also considered as one of the advantages of EVs for the application as drug delivery carriers to macrophages.

In chapter 1, I developed IL4-carrying sEVs by using genetic engineering, which enhanced anti-inflammatory effect of IL4 on macrophages. sEVs efficiently delivered IL4 to the synovial macrophages in arthritis model mice, and exhibited high anti-arthritis effect by modulating the macrophage polarization.

To investigate the potential of sEVs as an intracellular delivery carrier of therapeutic peptides to macrophages, in chapter 2, I developed sEVs internally loaded NF-κB inhibitor peptides. Also, to examine the relationship between the amount of cargoes in sEVs and pharmacological effect, I constructed sEVs loaded with different number of peptides. NF-κB inhibition and following anti-inflammatory effect on macrophages were investigated. Since only sEVs multiply loaded with peptides demonstrated NF-κB inhibitory effect, I found that the amount of cargoes in sEVs was significant factor for obtaining pharmacological effect of cargoes.

In chapter 3, based on the findings of chapter 2, I initially constructed an efficient method of cargo loading into lEVs. Using the established method, I developed lEVs multiply loaded with therapeutic peptides. lEVs successfully delivered the peptides into the macrophage cytosol, and modulated the activation of tumor associated macrophages. Furthermore, combination therapy of PD-1 blockade + peptide-loaded lEVs displayed favorable anti-cancer effect, suggesting that the combination therapy can be a promising option for cancer treatment.

The findings in this thesis contribute to the development of macrophage-targeted EV-based therapies.

List of publications included in this thesis

Interleukin-4-carrying small extracellular vesicles with a high potential as anti-inflammatory therapeutics based on modulation of macrophage function

Biomaterials (2021 Nov), 278, 121160, doi: 10.1016/j.biomaterials.2021.121160

Intercellular delivery of NF-κB inhibitor peptide utilizing small extracellular vesicles for the application of anti-inflammatory therapy

J Control Release (2020 Dec), 10, 328, 435-443, doi: 10.1016/j.jconrel.2020.09.001

Development of an efficient peptide/protein loading method into extracellular vesicles using multivalent linked biotinylated proteins.

Manuscript in Preparation

Acknowledgements

First and foremost, I would like to express my deepest gratitude to Professor Yoshinobu Takakura, Ph.D. from the Department of Biopharmaceutics and Drug Metabolism, Graduate School of Pharmaceutical Sciences, Kyoto University for giving me the best opportunity to learn the excitement of pharmaceutical science and immense myself in the research of drug delivery system at his wonderful laboratory. All his insightful advice, warm support and encouragements enabled me to progress over the course of six years to gain my Ph.D. degree.

I would like to extend my sincere gratitude to Associate Professor Yuki Takahashi, Ph.D. from the Department of Biopharmaceutics and Drug Metabolism, for his patient assistance and advice. I would not have been able to solve difficulties and complete my Ph.D. course without his creative ideas, valuable discussion, unwavering guidance and encouragements.

In particular, I am deeply grateful to these two wonderful advisers, Dr. Takakura and Dr. Yuki Takahashi for accepting me as a doctorate student while working in the industry. I have felt how fortunate I am to be able to pursue my dreams under their guidance. They provided me continuous support, advice and encouragements, which always inspired me and gave me courage to keep moving forward.

I would like to thank Assistant Professor Yusuke Kawamoto, Ph.D. from the Department of Biopharmaceutics and Drug Metabolism for his advice and kind support.

I would like to thank all members of the Department of Biopharmaceutics and Drug Metabolism, both the alumni and current members, for the valuable discussions and experimental assistances, as well as memorable moments we have shared. I would like to give my special thanks to Ms. Noriko Hikihara, Dr. Atsushi Hamana, Dr. Shozo Ohtsuki, Dr. Aki Yamamoto, Dr. Wen Liu, Dr. Keisuke Umemura, Ms. Ayane Yabuta and Mr. Kodai Nakao for their advice and unstinting help.

Last but not least, I would like to thank my family for raising me, telling me essential life lessons, and providing me unparalleled assistances and care. I am truly grateful to them for always respecting my decisions and letting me pursue my aspirations. Their endless love and support allow me to move forward for a better world now and in the future.

References

[1] P. Krzyszczyk, R. Schloss, A. Palmer, F. Berthiaume, The role of macrophages in acute and chronic wound healing and interventions to promote pro-wound healing phenotypes, Front. Physiol. 9 (2018) 1–22. https://doi.org/10.3389/fphys.2018.00419.

[2] E. Woith, G. Fuhrmann, M.F. Melzig, Molecular Sciences Extracellular Vesicles-Connecting Kingdoms, Int. J. Mol. Sci. 20 (2019) 5695.

[3] M. Tkach, C. Théry, Communication by Extracellular Vesicles: Where We Are and Where We Need to Go, Cell. 164 (2016) 1226–1232. https://doi.org/10.1016/j.cell.2016.01.043.

[4] J. Kowal, M. Tkach, C. Théry, Biogenesis and secretion of exosomes, Curr. Opin. Cell Biol. 29 (2014) 116–125. https://doi.org/10.1016/j.ceb.2014.05.004.

[5] G. Van Niel, G. D'Angelo, G. Raposo, Shedding light on the cell biology of extracellular vesicles, Nat. Rev. Mol. Cell Biol. 19 (2018) 213–228. https://doi.org/10.1038/nrm.2017.125.

[6] T. Imai, Y. Takahashi, M. Nishikawa, K. Kato, M. Morishita, T. Yamashita, A. Matsumoto, C. Charoenviriyakul, Y. Takakura, Macrophage-dependent clearance of systemically administered B16BL6-derived exosomes from the blood circulation in mice, J. Extracell. Vesicles. 4 (2015) 1–8. https://doi.org/10.3402/jev.v4.26238.

[7] A. Matsumoto, Y. Takahashi, M. Nishikawa, K. Sano, M. Morishita, C. Charoenviriyakul, H. Saji, Y. Takakura, Role of Phosphatidylserine-Derived Negative Surface Charges in the Recognition and Uptake of Intravenously Injected B16BL6-Derived Exosomes by Macrophages, J. Pharm. Sci. 106 (2017) 168–175. https://doi.org/10.1016/j.xphs.2016.07.022.

[8] D.B. Nguyen, T.B. Thuy Ly, M.C. Wesseling, M. Hittinger, A. Torge, A. Devitt, Y. Perrie, I. Bernhardt, Characterization of microvesicles released from human red blood cells, Cell. Physiol. Biochem. 38 (2016) 1085–1099. https://doi.org/10.1159/000443059.

[9] M. Xu, Q. Yang, X. Sun, Y. Wang, Recent Advancements in the Loading and Modification of Therapeutic Exosomes, Front. Bioeng. Biotechnol. 8 (2020). https://doi.org/10.3389/fbioe.2020.586130.

[10] A. Mantovani, A. Sica, S. Sozzani, P. Allavena, A. Vecchi, M. Locati, The chemokine system in diverse forms of macrophage activation and polarization, Trends Immunol. 25 (2004) 677–686. https://doi.org/10.1016/j.it.2004.09.015.

[11] J.F. Rossi, Z.Y. Lu, M. Jourdan, B. Klein, Interleukin-6 as a therapeutic target, Clin. Cancer Res. 21 (2015) 1248–1257. https://doi.org/10.1158/1078-0432.CCR-14-2291.

[12] C. Monaco, J. Nanchahal, P. Taylor, M. Feldmann, Anti-TNF therapy: Past, present and future, Int. Immunol. 27 (2015) 55–62. https://doi.org/10.1093/intimm/dxu102.

[13] W. Ohashi, K. Hattori, Y. Hattori, Control of macrophage dynamics as a potential therapeutic approach for clinical disorders involving chronic inflammation, J. Pharmacol. Exp. Ther. 354 (2015) 240–250. https://doi.org/10.1124/jpet.115.225540.

[14] I.G. Luzina, A.D. Keegan, N.M. Heller, G.A.W. Rook, T. Shea-Donohue, S.P. Atamas, Regulation of inflammation by interleukin-4: a review of "alternatives," J. Leukoc. Biol. 92 (2012) 753–764. https://doi.org/10.1189/jlb.0412214.

[15] J.B. Allen, H.L. Wong, G.L. Costa, M.J. Bienkowski, S.M. Wahl, Suppression of monocyte function and differential regulation of IL-1 and IL-1ra by IL-4 contribute to resolution of experimental arthritis., J. Immunol. 151 (1993) 4344–51. http://www.ncbi.nlm.nih.gov/pubmed/8409406.

[16] K. Ghoreschi, P. Thomas, S. Breit, M. Dugas, R. Mailhammer, W. Van Eden, R. Van der Zee, T. Biedermann, J. Prinz, M. Mack, U. Mrowietz, E. Christophers, D. Schlöndorff, G. Plewig, C.A. Sander, M. Rocken, Interleukin-4 therapy of psoriasis induces Th2 responses and improves human autoimmune disease, Nat. Med. 9 (2003) 40–46. https://doi.org/10.1038/nm804.

[17] E. Lubberts, L.A.B. Joosten, M. Chabaud, L. Van Den Bersselaar, B. Oppers, C.J.J. Coenen-De Roo, C.D. Richards, P. Miossec, W.B. Van Den Berg, IL-4 gene therapy for collagen arthritis suppresses synovial IL-17 and osteoprotegerin ligand and prevents bone erosion, J. Clin. Invest. 105 (2000) 1697–1710. https://doi.org/10.1172/JCI7739.

[18] L.A.B. Joosten, E. Lubberts, P. Durez, M.M.A. Helsen, M.J.M. Jacobs, M. Goldman, W.B. Van den Berg, Role of interleukin-4 and interleukin-10 in murine collagen-induced arthritis: Protective effect of interleukin-4 and interleukin-10 treatment on cartilage destruction, Arthritis Rheum. 40 (1997) 249–260. https://doi.org/10.1002/art.1780400209.

[19] L.A.B. Joosten, E. Lubberts, M.M.A. Helsen, T. Saxne, C.J.J. Coenen-De Roo, D. Heinegård, W.B. Van Den Berg, Protection against cartilage and bone destruction by systemic interleukin-4 treatment in established murine type II collagen-induced arthritis, Arthritis Res. 1 (1999) 81–91. https://doi.org/10.1186/ar14.

[20] E. Lubberts, L.A. Joosten, L. van Den Bersselaar, M.M. Helsen, A.C. Bakker, J.B. van Meurs, F.L. Graham, C.D. Richards, W.B. van Den Berg, Adenoviral vector-mediated overexpression of IL-4 in the knee joint of mice with collagen-induced arthritis prevents cartilage destruction., J. Immunol. 163 (1999) 4546–56. http://www.ncbi.nlm.nih.gov/pubmed/10510398.

[21] J.Prendivill; N. Thatcher; M. Lind; R. McIntosh; A. Ghosh; P. Stern; D. Crowther, Recombinant human interleukin-4 (rhu IL-4) administered by the intravenous and subcutaneous routes in patients with advanced cancer—A phase I toxicity study and pharmacokinetic analysis, Eur. J. Cancer. 29 (1993) 1700–1707.

[22] J.A. Sosmon; S.G. Fisher; C.Kwfer; R.I.Fisher; T.M.Ellis, A phase I trial of continuous infusion interleukin-4 (IL-4) alone and following interleukin-2 (IL2) in cancer patients, Ann. Oncol. (1994) 447–452.

[23] J. Lundin, E. Kimby, L. Bergmann, T. Karakas, H. Mellstedt, A. Österborg, Interleukin 4 therapy for patients with chronic lymphocytic leukaemia: A phase I/II study, Br. J. Haematol. 112 (2001) 155–160. https://doi.org/10.1046/j.1365-2141.2001.02525.x.

[24] P. Dasgupta, A.D. Keegan, Contribution of alternatively activated macrophages to allergic lung inflammation: A tale of mice and men, J. Innate Immun. 4 (2012) 478–488. https://doi.org/10.1159/000336025.

[25] H. Gandhi, R. Worch, K. Kurgonaite, M. Hintersteiner, P. Schwille, C. Bökel, T. Weidemann, Dynamics and interaction of Interleukin-4 receptor subunits in living cells, Biophys. J. 107 (2014) 2515–2527. https://doi.org/10.1016/j.bpj.2014.07.077.

[26] K. Kurgonaite, H. Gandhi, T. Kurth, S. Pautot, P. Schwille, T. Weidemann, C. Bökel, Essential role of endocytosis for interleukin-4-receptor-mediated JAK/STAT signalling, J. Cell Sci. 128 (2015) 3781–3795. https://doi.org/10.1242/jcs.170969.

[27] L.A. Mulcahy, R.C. Pink, D.R.F. Carter, Routes and mechanisms of extracellular vesicle uptake, J. Extracell. Vesicles. 3 (2014) 1–14. https://doi.org/10.3402/jev.v3.24641.

[28] K. Umemura, S. Ohtsuki, M. Nagaoka, K. Kusamori, T. Inoue, Y. Takahashi, Y. Takakura, M. Nishikawa, Critical contribution of macrophage scavenger receptor 1 to the uptake of nanostructured DNA by immune cells, Nanomedicine. (2021). https://doi.org/10.1016/j.nano.2021.102386.

[29] Y. Takahashi, M. Nishikawa, H. Shinotsuka, Y. Matsui, S. Ohara, T. Imai, Y. Takakura, Visualization and in vivo tracking of the exosomes of murine melanoma B16-BL6 cells

in mice after intravenous injection, J. Biotechnol. 165 (2013) 77–84. https://doi.org/10.1016/j.jbiotec.2013.03.013.

[30] C. Charoenviriyakul, Y. Takahashi, M. Morishita, M. Nishikawa, Y. Takakura, Role of Extracellular Vesicle Surface Proteins in the Pharmacokinetics of Extracellular Vesicles, Mol. Pharm. 15 (2018) 1073–1080. https://doi.org/10.1021/acs.molpharmaceut.7b00950.

[31] M. Morishita, Y. Takahashi, A. Matsumoto, M. Nishikawa, Y. Takakura, Exosome-based tumor antigens–adjuvant co-delivery utilizing genetically engineered tumor cell-derived exosomes with immunostimulatory CpG DNA, Biomaterials. 111 (2016) 55–65. https://doi.org/10.1016/j.biomaterials.2016.09.031.

[32] M. Morishita, Y. Takahashi, A. Matsumoto, M. Nishikawa, Y. Takakura, Exosome-based tumor antigens–adjuvant co-delivery utilizing genetically engineered tumor cell-derived exosomes with immunostimulatory CpG DNA, Biomaterials. 111 (2016) 55–65. https://doi.org/10.1016/j.biomaterials.2016.09.031.

[33] D.G. You, G. Saravanakumar, S. Son, H.S. Han, R. Heo, K. Kim, I.C. Kwon, J.Y. Lee, J.H. Park, Dextran sulfate-coated superparamagnetic iron oxide nanoparticles as a contrast agent for atherosclerosis imaging, Carbohydr. Polym. 101 (2014) 1225–1233. https://doi.org/10.1016/j.carbpol.2013.10.068.

[34] D.C. Watson, D. Bayik, A. Srivatsan, C. Bergamaschi, A. Valentin, G. Niu, J. Bear, M. Monninger, M. Sun, A. Morales-Kastresana, J.C. Jones, B.K. Felber, X. Chen, I. Gursel, G.N. Pavlakis, Efficient production and enhanced tumor delivery of engineered extracellular vesicles, Biomaterials. 105 (2016) 195–205. https://doi.org/10.1016/j.biomaterials.2016.07.003.

[35] D.B. Thompson, R. Villaseñor, B.M. Dorr, M. Zerial, D.R. Liu, Cellular uptake mechanisms and endosomal trafficking of supercharged proteins, Chem. Biol. 19 (2012) 831–843. https://doi.org/10.1016/j.chembiol.2012.06.014.

[36] J. Li, H.C. Hsu, J.D. Mountz, Managing macrophages in rheumatoid arthritis by reform or removal, Curr. Rheumatol. Rep. 14 (2012) 445–454. https://doi.org/10.1007/s11926-012-0272-4.

[37] M. Mendt, K. Rezvani, E. Shpall, Mesenchymal stem cell-derived exosomes for clinical use, Bone Marrow Transplant. 54 (2019) 789–792. https://doi.org/10.1038/s41409-019-0616-z.

[38] Hui Zhao; Qianwen; Zhenzhen Pan; Yang Bai; Zequn Li; Huiying Zhang; Qiu Zhang;

Chun Guo; Lining Zhang; Qun Wang, Exosomes From Adipose-Derived Stem Cells Attenuate Adipose Inflammation and Obesity Through Polarizing M2 Macrophages and Beiging in White Adipose Tissue, 67 (n.d.) 235–247.

[39] H. Kim, S.Y. Wang, G. Kwak, Y. Yang, I.C. Kwon, S.H. Kim, Exosome-Guided Phenotypic Switch of M1 to M2 Macrophages for Cutaneous Wound Healing, Adv. Sci. 6 (2019). https://doi.org/10.1002/advs.201900513.

[40] Y. Yang, X. Hu, L. Cheng, W. Tang, W. Zhao, Y. Yang, J. Zuo, Periplocoside A ameliorated type II collagen-induced arthritis in mice via regulation of the balance of Th17/Treg cells, Int. Immunopharmacol. 44 (2017) 43–52. https://doi.org/10.1016/j.intimp.2016.12.013.

[41] S. Gordon, Alternative activation of macrophages, Nat. Rev. Immunol. 3 (2003) 23–35. https://doi.org/10.1038/nri978.

[42] R.L. Gieseck, M.S. Wilson, T.A. Wynn, Type 2 immunity in tissue repair and fibrosis, Nat. Rev. Immunol. 18 (2018) 62–76. https://doi.org/10.1038/nri.2017.90.

[43] N.J. Horwood, Macrophage Polarization and Bone Formation: A review, Clin. Rev. Allergy Immunol. 51 (2016) 79–86. https://doi.org/10.1007/s12016-015-8519-2.

[44] S. Chen, H. Liang, Y. Ji, H. Kou, C. Zhang, G. Shang, C. Shang, Z. Song, L. Yang, L. Liu, Y. Wang, H. Liu, Curcumin Modulates the Crosstalk Between Macrophages and Bone Mesenchymal Stem Cells to Ameliorate Osteogenesis, Front. Cell Dev. Biol. 9 (2021) 1–13. https://doi.org/10.3389/fcell.2021.634650.

[45] C. Guder, S. Gravius, C. Burger, D.C. Wirtz, F.A. Schildberg, Osteoimmunology: A Current Update of the Interplay Between Bone and the Immune System, Front. Immunol. 11 (2020) 1–19. https://doi.org/10.3389/fimmu.2020.00058.

[46] R.G. Baker, M.S. Hayden, S. Ghosh, NF-κB, inflammation, and metabolic disease, Cell Metab. 13 (2011) 11–22. https://doi.org/10.1016/j.cmet.2010.12.008.

[47] P. Viatour, M.P. Merville, V. Bours, A. Chariot, Phosphorylation of NF-κB and IκB proteins: Implications in cancer and inflammation, Trends Biochem. Sci. 30 (2005) 43–52. https://doi.org/10.1016/j.tibs.2004.11.009.

[48] P.P. Tak, G.S. Firestein, NF-κB: A key role in inflammatory diseases, J. Clin. Invest. 107 (2001) 7–11. https://doi.org/10.1172/JCI11830.

[49] N. Wang, H. Liang, K. Zen, Molecular mechanisms that influence the macrophage M1-M2 polarization balance, Front. Immunol. 5 (2014) 1–9.

https://doi.org/10.3389/fimmu.2014.00614.

[50] M.J. May, F. D'Acquisto, L.A. Madge, J. Glockner, J.S. Pober, S. Ghosh, Selective inhibition of NF-κB activation by a peptide that blocks the interaction of NEMO with the IκB kinase complex, Science (80-.). 289 (2000) 1550–1554. https://doi.org/10.1126/science.289.5484.1550.

[51] M.J. May, R.B. Marienfeld, S. Ghosh, Characterization of the IκB-kinase NEMO binding domain, J. Biol. Chem. 277 (2002) 45992–46000. https://doi.org/10.1074/jbc.M206494200.

[52] S. Ghosh, M. Karin, Missing pieces in the NF-κB puzzle, Cell. 109 (2002) 81–96. https://doi.org/10.1016/S0092-8674(02)00703-1.

[53] I. Stancovski, D. Baltimore, NF-κB Activation: The IκB Kinase Revealed?, Cell. 91 (1997) 299–302.

[54] T. Huxford, G. Ghosh, A structural guide to proteins of the NF-kappaB signaling module., Cold Spring Harb. Perspect. Biol. 1 (2009) 1–16. https://doi.org/10.1101/cshperspect.a000075.

[55] M. Karin, M. Delhase, The IκB kinase (IKK) and NF-κB: Key elements of proinflammatory signalling, Semin. Immunol. 12 (2000) 85–98. https://doi.org/10.1006/smim.2000.0210.

[56] S. Dai, T. Hirayama, S. Abbas, Y. Abu-Amer, The IκB kinase (IKK) inhibitor, NEMO-binding domain peptide, blocks osteoclastogenesis and bone erosion in inflammatory arthritis, J. Biol. Chem. 279 (2004) 37219–37222. https://doi.org/10.1074/jbc.C400258200.

[57] S.W. Tas, M.J. Vervoordeldonk, N. Hajji, M.J. May, S. Ghosh, P.P. Tak, Local treatment with the selective IκB kinase β inhibitor NEMO-binding domain peptide ameliorates synovial inflammation, Arthritis Res. Ther. 8 (2006) 1–9. https://doi.org/10.1186/ar1958.

[58] W. Shibata, S. Maeda, Y. Hikiba, A. Yanai, T. Ohmae, K. Sakamoto, H. Nakagawa, K. Ogura, M. Omata, Cutting Edge: The IκB Kinase (IKK) Inhibitor, NEMO-Binding Domain Peptide, Blocks Inflammatory Injury in Murine Colitis, J. Immunol. 179 (2007) 2681–2685. https://doi.org/10.4049/jimmunol.179.5.2681.

[59] D. Sun, Z. Xiaoying, X. Xiang, Y. Liu, S. Zhang, C. Liu, S. Barnes, W. Grizzle, D. Miller, H.-G. Zhang, A Novel Nanoparticle Drug Delivery System: The Anti-

inflammatory Activity of Curcumin Is Enhanced When Encapsulated in Exosomes, Mol. Ther. 18 (2010) 1606–1614.

[60] M. Haney, N. Klyachko, Y. Zhao, R. Gupta, E. Plotnikova, Z. He, T. Patel, A. Piroyan, M. Sokolsky, A. Kabanov, E. Batrakova, Exosomes as Drug Delivery Vehicles for Parkinson's Disease Therapy, J. Control. Release. 207 (2015) 18–30. https://doi.org/10.1016/j.physbeh.2017.03.040.

[61] D.E. Murphy, O.G. de Jong, M. Brouwer, M.J. Wood, G. Lavieu, R.M. Schiffelers, P. Vader, Extracellular vesicle-based therapeutics: natural versus engineered targeting and trafficking, Exp. Mol. Med. 51 (2019). https://doi.org/10.1038/s12276-019-0223-5.

[62] Y. Arima, W. Liu, Y. Takahashi, M. Nishikawa, Y. Takakura, Effects of Localization of Antigen Proteins in Antigen-Loaded Exosomes on Efficiency of Antigen Presentation, Mol. Pharm. 16 (2019) 2309–2314. https://doi.org/10.1021/acs.molpharmaceut.8b01093.

[63] C. Charoenviriyakul, Y. Takahashi, M. Morishita, M. Nishikawa, Y. Takakura, Role of Extracellular Vesicle Surface Proteins in the Pharmacokinetics of Extracellular Vesicles, Mol. Pharm. 15 (2018) 1073–1080. https://doi.org/10.1021/acs.molpharmaceut.7b00950.

[64] Y. Hayakawa, S. Maeda, H. Nakagawa, Y. Hikiba, W. Shibata, K. Sakamoto, A. Yanai, Y. Hirata, K. Ogura, S. Muto, A. Itai, M. Omata, Effectiveness of IκB kinase inhibitors in murine colitis-associated tumorigenesis, J. Gastroenterol. 44 (2009) 935–943. https://doi.org/10.1007/s00535-009-0098-7.

[65] R.S. Jope, C.J. Yuskaitis, E. Beurel, Glycogen Synthase Kinase-3 (GSK3): Inflammation, Diseases, and Therapeutics, Neurochem. Res. 32 (2007) 577–595. https://www.ncbi.nlm.nih.gov/pmc/articles/PMC1970866/pdf/nihms24923.pdf%0Ahttp://www.ncbi.nlm.nih.gov/pubmed/16944320.

[66] M. Maqbool, M. Mobashir, N. Hoda, Pivotal role of glycogen synthase kinase-3: A therapeutic target for Alzheimer's disease, Eur. J. Med. Chem. 107 (2016) 63–81. https://doi.org/10.1016/j.ejmech.2015.10.018.

[67] M.A. Bogoyevitch, I. Boehm, A. Oakley, A.J. Ketterman, R.K. Barr, Targeting the JNK MAPK cascade for inhibition: Basic science and therapeutic potential, Biochim. Biophys. Acta - Proteins Proteomics. 1697 (2004) 89–101. https://doi.org/10.1016/j.bbapap.2003.11.016.

[68] B. Hu, L. Xu, Y. Li, X. Bai, M. Xing, Q. Cao, H. Liang, S. Song, A. Ji, A Peptide Inhibitor of Macrophage Migration in Atherosclerosis Purified From the Leech

Whitmania Pigra, J. Ethnopharmacol. (2020). https://doi.org/10.1016/j.jep.2020.112723.

[69] M.N. Rahimi, L.K. Buckton, S.S. Zaiter, J. Kho, V. Chan, A. Guo, J. Konesan, S. Kwon, L.K.O. Lam, M.F. Lawler, M. Leong, G.D. Moldovan, D.A. Neale, G. Thornton, S.R. McAlpine, Synthesis and Structure-Activity Relationships of Inhibitors That Target the C-Terminal MEEVD on Heat Shock Protein 90, ACS Med. Chem. Lett. 9 (2018) 73–77. https://doi.org/10.1021/acsmedchemlett.7b00310.

[70] M.N. Rahimi, S.R. McAlpine, Protein-protein inhibitor designed de novo to target the MEEVD region on the C-terminus of Hsp90 and block co-chaperone activity, Chem. Commun. 55 (2019) 846–849. https://doi.org/10.1039/C8CC07576J.

[71] S. Sueda, Y.Q. Li, H. Kondo, Y. Kawarabayasi, Substrate specificity of archaeon Sulfolobus tokodaii biotin protein ligase, Biochem. Biophys. Res. Commun. 344 (2006) 155–159. https://doi.org/10.1016/j.bbrc.2006.03.118.

[72] S. Sueda, S. Yoneda, H. Hayashi, Site-Specific Labeling of Proteins by Using Biotin Protein Ligase Conjugated with Fluorophores, ChemBioChem. 12 (2011) 1367–1375. https://doi.org/10.1002/cbic.201000738.

[73] S. Suman, P.K. Sharma, G. Rai, S. Mishra, D. Arora, P. Gupta, Y. Shukla, Current perspectives of molecular pathways involved in chronic inflammation-mediated breast cancer, Biochem. Biophys. Res. Commun. 472 (2016) 401–409. https://doi.org/10.1016/j.bbrc.2015.10.133.

[74] Q. Wu, W. Zhou, S. Yin, Y. Zhou, T. Chen, J. Qian, R. Su, L. Hong, H. Lu, F. Zhang, H. Xie, L. Zhou, S. Zheng, Blocking Triggering Receptor Expressed on Myeloid Cells-1-Positive Tumor-Associated Macrophages Induced by Hypoxia Reverses Immunosuppression and Anti-Programmed Cell Death Ligand 1 Resistance in Liver Cancer, Hepatology. 70 (2019) 198–214. https://doi.org/10.1002/hep.30593.

[75] A.N. Chamseddine, T. Assi, O. Mir, S. Chouaib, Modulating tumor-associated macrophages to enhance the efficacy of immune checkpoint inhibitors: A TAM-pting approach, Pharmacol. Ther. 231 (2022) 107986. https://doi.org/10.1016/j.pharmthera.2021.107986.

[76] D.G. DeNardo, B. Ruffell, Macrophages as regulators of tumour immunity and immunotherapy, Nat. Rev. Immunol. 19 (2019) 369–382. https://doi.org/10.1038/s41577-019-0127-6.

[77] Y.R. Na, J.W. Kwon, D.Y. Kim, H. Chung, J. Song, D. Jung, H. Quan, D. Kim, J.S.

Kim, Y.W. Ju, W. Han, H.S. Ryu, Y.S. Lee, J.J. Hong, S.H. Seok, Protein Kinase A Catalytic Subunit Is a Molecular Switch that Promotes the Pro-tumoral Function of Macrophages, Cell Rep. 31 (2020) 107643. https://doi.org/10.1016/j.celrep.2020.107643.

[78] K. Takaishi, Y. Komohara, H. Tashiro, H. Ohtake, T. Nakagawa, H. Katabuchi, M. Takeya, Involvement of M2-polarized macrophages in the ascites from advanced epithelial ovarian carcinoma in tumor progression via Stat3 activation, Cancer Sci. 101 (2010) 2128–2136. https://doi.org/10.1111/j.1349-7006.2010.01652.x.

[79] C. Liu, P. Ke, J. Zhang, X. Zhang, X. Chen, Protein Kinase Inhibitor Peptide as a Tool to Specifically Inhibit Protein Kinase A, Front. Physiol. 11 (2020). https://doi.org/10.3389/fphys.2020.574030.

[80] U. Bharadwaj, M.M. Kasembeli, D.J. Tweardy, STAT3 Inhibitors in Cancer: A Comprehensive Update, 2016. https://doi.org/10.1007/978-3-319-42949-6_5.

[81] N. Takiguchi, Y. Takahashi, M. Nishikawa, Y. Matsui, Y. Fukuhara, D. Oushiki, K. Kiyose, K. Hanaoka, T. Nagano, Y. Takakura, Positive correlation between the generation of reactive oxygen species and activation/reactivation of transgene expression after hydrodynamic injections into mice, Pharm. Res. 28 (2011) 702–711. https://doi.org/10.1007/s11095-010-0331-3.